Title: High-throughput imaging of GABA fluorescence as a functional assay for variants in the neurodevelopmental gene, *SLC6A1*

Authors: Christopher Michael McGraw[1,2,3†], Guoqi Zhang[2], Gillian Prinzing[4], Kimberly Wiltrout[4], Annapurna Poduri[2,4†,5]

Affiliations

[1]Department of Neurology, Massachusetts General Hospital, Harvard Medical School, Boston, MA 02115, USA

[2]Department of Neurology, The F.M. Kirby Neurobiology Center, Boston Children's Hospital, Harvard Medical School, Boston, MA 02115, USA

[3]Department of Neurology, Feinberg School of Medicine, Northwestern University, Chicago, IL 60611, USA

[4]Department of Neurology, Boston Children's Hospital; Harvard Medical School, Boston, MA 02115, USA

[5]National Institutes of Neurological Disorders and Stroke, NIH, Bethesda, MD, USA

[†]Author's current affiliation.

Correspondence to:

Christopher Michael McGraw, MD, PhD

Department of Neurology, Feinberg School of Medicine, Northwestern University, Chicago, IL 60611, USA

E-mail: christopher.mcgraw@northwestern.edu

Abstract (200 words)

Pathogenic variants in *SLC6A1*, which encodes GABA Transporter 1 (GAT-1), are associated with developmental delay, autism, epilepsy (e.g., epilepsy with myoclonic astatic seizures [EMAS]), and possibly schizophrenia. Functional assays to establish pathogenicity of human variants is a key limiting factor in the clinical interpretation of genetic findings. Methods based on radioactive [3H]-GABA uptake come with significant regulatory concerns, cost, and workflow complexity, which could be resolved by an

alternate assay. To address this issue, we developed a high-content fluorescence imaging assay of GAT-1-mediated GABA uptake using a genetically encoded GABA sensor, iGABA-Snfr. We demonstrated that pathogenic variants strongly reduced uptake (mean, -89.4% [95% CI, -71.5% to -107.3%]). Some variants of uncertain significance (VUS) were associated with reduced GABA uptake (G111R, S459R, V511M; mean, -101.2% [95% CI -81.1% to -121.3%]), whereas others showed only mild reduction (R211C, R566H, F242V, R419C; mean, -33.6% [95% CI -17.2% to -50.1%]), supporting variant reclassification. Variant-specific effects on iGABA were highly correlated with the results of the radioactive [3H]-GABA assay (R^2=0.8095, p<0.0001). The molecular chaperone 4-phenylbutyric acid (4PBA) was associated with ~35% increase in iGABA. This non-radioactive assay is suitable for functional validation and high-throughput screening to identify positive modulators of GAT-1.

1. Introduction

The gamma-aminobutyric acid (GABA) transporter 1 (GAT-1), encoded by *SLC6A1*, plays a critical role in regulating extracellular GABA levels in the central nervous system (Richerson & Wu, 2004; Wu et al., 2007), thereby modulating inhibitory neurotransmission. Monoallelic variants in *SLC6A1* are associated with a spectrum of neurological disorders, including epilepsy, intellectual disability, autism spectrum disorder, and possibly schizophrenia (Cai et al., 2019; Carvill et al., 2015; Johannesen et al., 2018; Mattison et al., 2018; Silva et al., 2024). Most pathogenic variants have been shown to result in loss of function as evidenced by functional assays (Silva et al., 2024). The mechanism of GAT-1 haploinsufficiency involves reduced GABA transport due to variant-specific effects on GAT-1 activity (Mattison et al., 2018; Silva et al., 2024) as well as reduced GAT-1 surface expression (Cai et al., 2019; Nwosu et al., 2022; Silva et al., 2024) via protein destabilization and ER retention (Cai et al., 2019). Agonists of GAT-1 have not yet been identified. However, the molecular chaperone 4-phenylbutyric acid (4PBA) has shown therapeutic potential in S*lc6a1* mouse models (reduced spike-wave discharges) concomitant with increased GAT-1 surface expression and GABA uptake(Nwosu et al., 2022).

59 Functional assays are essential for evaluating the impact of variants on GAT-1 function
60 and for reclassifying VUS to guide clinical management. Traditional methods for
61 assessing GAT-1 function rely on radioactive [^{3}H]-GABA uptake assays(Cai et al., 2019;
62 Nwosu et al., 2022; Silva et al., 2024). While effective, radioactivity-based assays are
63 burdened by regulatory restrictions and high waste disposal costs (Eglen & Reisine,
64 2009), making them less suitable for modern high-throughput applications such as high-
65 content imaging.

66 To address these challenges, we developed a novel, non-radioactive, cell-based assay
67 for GAT-1 function utilizing the genetically encoded GABA fluorescence sensor (iGABA-
68 Snfr(Marvin et al., 2019) aka "iGABA") coupled with high-throughput automated
69 microscopy. The objectives of this study were two-fold: first, to validate the iGABA
70 assay for assessing the functional impact of *SLC6A1* variants, including a novel
71 missense variant M55T; and second, to demonstrate the assay's suitability for high-
72 throughput drug screening to identify positive modulators of GAT-1 activity. The GAT-1
73 iGABA assay provides a versatile platform for both variant classification and therapeutic
74 development for SLC6A1-related disorders.

75 **2. Materials and methods.**

76 **2.1. Construction of hGAT1 and iGABA-Snfr expression vectors.** To construct the
77 hGAT1-P2A-tdTomato vector, the following sequences were amplified from the
78 indicated sources by PCR: 1) full-length hGAT1 cDNA sequence without the final stop
79 codon (1835 nts) from human clone (R&D Systems, hGAT-1/SLC6A1 VersaClone
80 cDNA, RDC1033; Accession: NP_003033); 2) a 79-nt length P2A sequence from
81 SID4x-dCas9-KRAB (AddGene 106399), and 3) tdTomato (1468 nts) from ptwB
82 (AddGene 48735). Fragments were combined with the pCDNA3.1 vector (NeoR/KanR,
83 AmpR) targeting the MCS by InFusion cloning (Takara) to generate an 8.6kB vector (→
84 "V006-2").
85 To construct an iGABA-Snfr-P2A-mBFP vector suitable for a cell-based assay, the
86 following sequences were amplified from the indicated sources by PCR: 1) the CDS of
87 iGABA-Snfr-F102Y-Y137L without the final stop codon (1976 nts) was amplified from
88 pAAV-GFAP-iGABASnFR_F102Y_Y137L (Addgene #112174); 2) a 796 nt fragment

89 containing P2A-mTagBFP2 was amplified from lentiGuide-Hygro-mTagBFP2
90 (AddGene# 99374). Fragments were combined with the pCDNA3.1 vector targeting the
91 MCS by InFusion cloning to generate a 7.9kB vector (→ "V007-2"). Subsequently, to
92 abrogate surface expression, the 5' IgG K-leader site was removed (InFusion) while
93 retaining the start codon, and the 3' terminal PDGFR site was removed, to yield a 7.8kB
94 vector pCDNA3.1_iGABA-Snfr-F102Y-Y137L del IgGK del PDGFR T2A mBFP (→
95 "V007-2.2"). Final vectors were Sanger sequenced through the coding sequences.

96 **2.2. Generation of hGAT1 deletion constructs and human variant hGAT1**
97 **constructs.** For deletion constructs, three sets of primers were designed to remove the
98 extracellular domain (ECD; amino acids 145-211), cytoplasmic domain (CPD; amino
99 acids 1-52), and transmembrane domains 6-7 (TM6-7, amino acids 292-342) based on
100 Uniprot P30531. Representative human variants affecting the GAT-1 coding sequence
101 were identified from ClinVar, gnomad, selected cohort studies(Carvill et al., 2015;
102 Johannesen et al., 2018; Mattison et al., 2018), and the SLC6A1-Portal (https://slc6a1-
103 portal.broadinstitute.org/, downloaded September 2022). Variants were selected based
104 on recurrence across individuals and distribution across predicted pathogenicity,
105 including variants classified as pathogenic/likely pathogenic (N= 7), benign/likely benign
106 (N=2), and uncertain significance (N= 7). Clinical details were downloaded on
107 September 8, 2022.

108 All variants are presented in **Table 1**. All primer sequences used for mutagenesis are
109 provided in **Supplementary Table 1**. Deletions and variants were introduced into GAT-
110 1 vector V006-2 by site-directed mutagenesis (InFusion Snap Assembly, Takara) and
111 KOD polymerase (Sigma, 71085) using the associated primers (IDT). Constructs were
112 verified by Sanger sequencing.
113

114 **2.3. Transient transfection assays of hGAT1 deletion and human variant**
115 **constructs.**
116 HeLa cells (ATCC, CCL-2) were maintained in T75 flasks with EMEM (Cat#112-212-
117 101, VWR Company) supplemented with 10% fetal bovine serum (FBS, Cat#16-000-04,
118 Gibco) and 1X penicillin-streptomycin (PS) and 2% L-Glutamine (Cat# 16777-162,
119 VWR) and incubated at 37°C with 5% CO2. For transient transfection, 2 million HeLa

120 cells were seeded into each 60 mm petri dish on day 1. On day 2, for each dish, 2.5ug
121 V007-2.2 and 2.5ug hGAT vector (WT or variant) (5ug total) were combined in 0.5mL
122 OptiMEM and mixed gently. Lipofectamine 2000 (Cat#52758, Invitrogen) 10uL was
123 diluted in 0.5mL OptiMEM. Diluted DNA and Lipofectamine were combined with gentle
124 mixing and incubated 20 minutes at room temperature. Finally, the 1mL was added to
125 each dish containing cells and 4mL of media, mixed gently by rocking back and forth,
126 then incubated for 4-6 hours before replacing media with EMEM complete media. On
127 day 3, transfected cells were dislodged by trypsin digest (Cat# 25300-054 from Gibco)
128 and seeded at 500k cells per well into 96 well plate (Greiner, 655090). After 6 hrs of
129 incubation, cells were washed twice with PBS and treated with 260 uM tiagabine (TGB;
130 Cat # T3165, Lot PQ2JD-NP from TCI) diluted in EMEM + 10%FBS + 1X PS overnight
131 (~16 hrs). On day 4, media was removed and cells washed twice with PBS, then treated
132 with gamma-aminobutyric acid (GABA) (Cat# A2129-100G, Sigma) diluted in EMEM at
133 various concentrations at various incubations (1-8hrs) at 37degC. Each plate was
134 subsequently imaged using the ImageXpress Micro (Molecular Devices).

135 **2.4. Generation of hGAT1; iGABA-Snfr stable cell line**. A stable HeLa cell line
136 (ATCC, CCL-2) harboring both constructs (V006 and V007) was generated serially by
137 transfection of linearized constructs (PvuI digest) followed by extended antibiotic
138 selection, FACS to select single fluorescent cells for monoclonal culture, followed by
139 FACS reassessment. A stable HeLa cell line was first established with V006-2 with
140 G418 selection. This cell line was then used to generate a double stable cell line. The
141 vector V007-2.2 was converted to exchange PuroR resistance cassette with the existing
142 NeoR/Kan cassette by InFusion (→ V007-2.3), but we failed to recover puromycin-
143 resistant clones after several attempts. The vector V007-2.2 was then converted to have
144 blasticidin resistance (→ V007-2.4), from which 4 double-positive clones were
145 successfully isolated by FACS, two of which grew well and retained double-
146 fluorescence by FACS after extended incubation with double selection using blastocidin
147 (1ug/mL) and G418 (200ug/mL). Clone #2 was used for all subsequent studies.
148

149 **2.5. 4PBA assay.** For testing 4-phenylbutyric acid (4PBA; Sigma P21005), the
150 compound was dissolved to 1205.8mM in DMSO (198mg/mL) to generate a parent

151 stock. GABA was prepared to 500mM (515.6mg in 2mL PBS) and further diluted to
152 generate 50X GABA stocks for each GABA condition. 4PBA-GABA stocks for each
153 condition were generated by diluting the parent 4PBA stock in EMEM (16.5uL into
154 6600uL EMEM) then combined with 50X GABA (161.7uL 4PBA + 3.3uL 50X GABA).
155 For 4PBA 3mM, the parent 4PBA stock (1205.8mM) was used, but for 4PBA 1mM, the
156 parent stock was first diluted to 400mM (DDW), then diluted in EMEM and combined
157 with 50X GABA, as before. Drug plates were assembled in 96-well format using Integra
158 Viaflow automatic multi-channel pipettors. On the day of testing, medium from prepared
159 cells was aspirated and 1X 4PBA-GABA stocks were transferred directly to cells and
160 incubated at 37degC for 6 hours prior to imaging.

161 **2.6. Assays with hGAT1; iGABA-Snfr stable cell line.** For assays using the hGAT1;
162 iGABA-Snfr double stable cell line, cells were seeded into 384-well plates ($5X10^4$ cells
163 per well) in EMEM supplemented with 10% FBS, 2% L-Glutamine, 1X PS, G418
164 (200ug/mL), and blastocidin (1ug/mL) and allowed to grow to 80% confluence. On day
165 1, cells were preincubated overnight with 260uM TGB in EMEM. On day 2, GABA stock
166 was diluted to 3X desired concentrations (10nm-5uM) in EMEM with 3X 0.1% DMSO on
167 a “drug plate”, while EMEM was dispensed to an “EMEM only” plate using the Multidrop
168 Combi dispenser (ThermoScientific). For GABA application, under semi-sterile
169 conditions, the Bravo liquid handler (Agilent) was used to wash cells 3X in 1X PBS and
170 then remove remaining PBS and apply 20uL from “DMEM only” and 10uL from “drug
171 plate”. Plates were incubated at 37degC for 1-6hrs, before imaging using the IXM.

172 **2.7. High-content imaging and automated analysis.** Widefield fluorescence imaging
173 was performed using the ImageXpress Micro (IXM) with 20X objective with the following
174 filters and exposure durations: DAPI (mBFP; 10msec), FITC (iGABA-Snfr; 20msec), and
175 TexasRed (tdTomato; 5msec). Image analysis was performed using Molecular Devices
176 software to select cells with mBFP intensity above local background 150, with
177 approximate width 5-50um. Per-cell average fluorescence values for mBFP, iGABA,
178 and tdTomato are subsequently reported for all sites and wells.

179 **2.8. In vitro assay of iGABA-Snfr fluorescence.** In vitro fluorescence measurements
180 were performed on a Tecan Spark plate reading fluorimeter at ~28°C with excitation at

485 nm (20 nm bandpass) and emission collected at 532 nm (20 nm bandpass). Concentrated purified and dialyzed iGABASnFR.F102Y.Y137L protein was diluted to 0.2 μM in PBS. GABA and decoy compounds were purchased from Sigma-Aldrich and prepared as 100 mM stocks in PBS. Titrations were performed by making serial dilutions (1:2) of the stock compound into PBS and adding 10 μl of that to 100 μl of 0.2 μM protein solution. Fluorescence was measured before addition of compound, and ΔF/F was calculated as (F(treatment) − F(initial))/F(initial). Controls were performed with circularly permuted super-folder GFP (cpSFGFP; PMID: 16369541).

2.9. Data analysis and statistics. Data from IXM was extracted either as per-cell average fluorescence values or per-well averages across variable numbers of sites (4-10 sites) and processed further in R, Excel, and/or GraphPad Prism.

For variant experiments (with k variants), fractional change in iGABA fluorescence, M, due to GABA application is calculated in relation to each variant's vehicle-treated control, as: $M_i = (F_{i,\ GABA} - F_{i,\ vehicle}) / F_{i,\ vehicle}$, where F is the group-wise average iGABA fluorescence (across wells), and i is an element of the 1,…, k variants. Standard deviations, s_i, were adjusted by: $s_{i_adj} = s_i / F_{i,\ vehicle}$. Normalization to WT was performed as: $M_{i_adj} = M_i / M_{WT}$, where M_{WT} is the fractional change in iGABA fluorescence for wild-type GAT-1 control. For %WT, $M_{i_adj\%} = M_{i_adj}$ X 100.

For stable cell line experiments, fractional change in iGABA fluorescence, M, due to GABA application is calculated (similar to above) in relation to vehicle-treated control, but with i as an element of 1, …, p levels of GABA concentration.

Statistical inference was performed in GraphPad Prism as described in the main text. For plate normalization using linear models, per-well average data was analyzed in R using a custom script. Linear models were fit using function *lm* (R package, *stats*) while linear mixed models were fit using function *lmer* (R package, *lme4*). Bootstrap simulation was performed in R using the mean and standard deviations for each control. The robust strictly standardized mean difference (RSSMD) was calculated by the uniformly minimum-variance unbiased estimator (UMVUE) method(Zhang, 2011).

3. Results

211 **3.1. Development of a cell-based assay for hGAT1 function using iGABA-Snfr**
212 **fluorescence.**

213 To detect changes in intracellular GABA mediated by hGAT1 after exogenous
214 application of GABA (**Fig. 1B**), we generated two vectors, one expressing human GAT-
215 1 (hGAT1) cDNA (Accession: NP_003033) stoichiometrically linked with the red
216 fluorescent fluorophore tdTomato (**Fig. 1A**) and another expressing modified iGABA-
217 Snfr stoichiometrically linked to the blue fluorescent fluorophore mTagBFP2
218 (abbreviated mBFP). We selected the HeLa cell line (ATCC, CC2) based on publicly
219 available RNA-seq data (2021 CCLE release; DepMap, ACH-001086) showing
220 undetectable expression of *SLC6A1* (GAT-1; 0 TPM) and low or undetectable
221 expression of other GABA transporters including *SLC6A13* (GAT-2; 0 TPM), *SLC6A11*
222 (GAT-3; 0 TPM); *SLC6A12* (BGT1; 0 TPM), and *SLC6A6* (TauT; 1-2 TPM). Using
223 automated high content fluorescence microscopy (ImageXpress Micro) and automated
224 image analysis (**Fig. 1C)**, we demonstrated the ability to assay levels of iGABA-Snfr
225 fluorescence from thousands of cells per condition in 96-well format with a significant
226 increase in average per-cell iGABA fluorescence in response to exogenous GABA
227 application (**Figure 1D-E).**

228 **3.2. Validation of relative change in per-cell GABA fluorescence as molecular**
229 **read-out of GABA transporter activity**

230 To benchmark the effects of null variants, we utilized deletion constructs targeting
231 domains previously demonstrated to be critical for GAT1-mediated GABA uptake (CPD,
232 ECD, TM6-7) (**Fig 2A**). We confirmed that deletion variants were associated with
233 significantly reduced iGABA fluorescence relative to wild-type across a 5-log range
234 (1μM to 10mM; **Fig 2B**). Expressed as normalized fractional change in iGABA (relative
235 to vehicle controls; **Fig 2C**) or normalized relative to wild-type (**Fig 2D**), the reduced
236 uptake in GABA appeared most specific at lower concentrations of extracellular GABA
237 (1-10uM, similar to GAT-1 Km ~3uM(Wu et al., 2007)). At higher concentrations (100
238 μM GABA), we observed ~30-40% of WT GABA uptake, which we hypothesized may
239 be due either to residual GAT-1 protein function or nonspecific lower affinity
240 mechanisms of uptake. To assess this question, we examined iGABA fluorescence in

241 cells without GAT-1 transfection ("no GAT1" controls). Surprisingly, we observed
242 significantly greater nonspecific GABA uptake in the absence of GAT-1 at both low
243 (1uM) and higher (100uM) GABA concentrations compared to deletion variants
244 (**Supplementary Fig 1**), suggesting active interference between GAT-1 deletion
245 constructs and unknown mechanisms mediating low-affinity GABA uptake in HeLa cells
246 (perhaps TauT, a low-affinity GABA transporter), despite undetectable GABA uptake by
247 these variants. To further optimize the assay, we tested the effect of overnight pre-
248 treatment with the GAT-1 selective inhibitor, tiagabine (TGB) followed by wash-out, and
249 showed increased fractional change in iGABA across all GABA concentrations
250 (**Supplementary Fig 2A**). We also tested a range of incubation durations and
251 demonstrated increasing uptake up to 6 hours post-treatment (**Supplementary Fig 2B**).
252 Based on these observations, we determined that TGB pretreatment followed by low
253 GABA concentration (1 μM) incubation x 6 hrs would be most suitable for further
254 experiments. We demonstrated that increased iGABA fluorescence under these
255 conditions could be detected robustly across replicates (robust SSMD >2, robust Z
256 prime >0.1; **Fig 2E**).

257 **3.3. GABA fluorescence provides a functional assessment of missense variants**
258 **in GABA transporters**

259 We next asked whether iGABA fluorescence could detect changes in GABA uptake
260 related to human missense variants in *SLC6A1*. For this purpose, we selected *SLC6A1*
261 variants associated with neurodevelopmental disorder and/or epilepsy (**Fig 3A**),
262 including 7 pathogenic or likely pathogenic variants (G75R, G232V, A288V, S295L,
263 V342M, A357V, G362R), two benign or likely benign variants (R195H, I322M), and 7
264 variants of uncertain significance (VUS;, G111R, R211C, F242V, R419C, S459R,
265 V511M, R566H, S574R). One of these variants (R211C) has also been associated with
266 schizophrenia(Rees et al., 2020). Together, these variants comprise 38.7% (n=12 of 31)
267 of all recurrent missense variants to date (Silva et al., 2024).

268 We introduced missense variants into hGAT1 by site-directed mutagenesis and
269 performed the iGABA assay following transient transfection. We observed consistent
270 reductions in normalized GABA uptake among pathogenic variants (**Fig 3B-C**) with -

271 89.4% mean reduction in iGABA (SD 17.1, 95% CI -71.5% to -107.3%; N=6). Using the
272 lower limit (95th CI) of pathogenic GABA uptake as a threshold, some VUS were
273 associated with reduced GABA uptake (G111R, S459R, V511M; mean reduction, -
274 101.2%, SD 8.10, 95% CI -81.1% to -121.3%, N=3), whereas others showed only mild
275 reduction (R211C, R566H, F242V, R419C; mean reduction, -33.6%, SD 10.4, 95% CI -
276 17.2% to -50.1%, N=4) (**Fig 3C**).

277 Test-retest analysis demonstrated that variant-specific iGABA was highly correlated
278 (R^2=0.8498, p<0.0001) between independent replicates (**Fig 3D**). Variant-specific
279 effects on iGABA are also highly correlated (R^2=0.65-0.81, p<0.0001) with previously
280 published measurements estimated by radioactive [^{3}H]-GABA transport assay(Silva et
281 al., 2024)(**Fig 3E**), suggesting that the iGABA method performs similarly to this gold-
282 standard method. Last, variant-specific reductions in iGABA correlate with several
283 pathogenicity prediction scores, including PolyPhen2 (R^2=0.49, p<0.0001; **Fig 3F.i**),
284 SIFT (R^2=0.42, p<0.0001; not shown), and AlphaMissense (R^2=0.7181, p<0.0001; **Fig**
285 **3F.ii**).

286 Radioactive assays estimate an instantaneous rate of GABA uptake (pmol/ug/min)
287 whereas the iGABA method estimates intracellular GABA as it approaches equilibrium,
288 reflecting the balance between rates of GABA uptake vs GABA removal due to
289 unspecified processes (metabolism, sequestration, efflux). To understand these
290 differences, we performed time-series analysis to assess whether a pathogenic variant
291 possessing some residual transporter activity (V342M) alters the rate of GABA uptake,
292 the steady state intracellular concentration of GABA, or both (**Fig 4A**). Based on a non-
293 linear fit of pseudo-first order kinetics, the pathogenic V342M variant reduced steady-
294 state GABA (Plateau: WT: 0.28, 95% CI 0.26-0.31, vs V342M: 0.11, 95% CI 0.087-
295 0.204; **Fig 4B**) but had no effect on the rate at which iGABA approached its variant-
296 specific steady-state (rate constant, K (min^{-1}): WT: 0.0126, 95% CI 0.008-0.020; V342M:
297 0.009, 95% CI 0.002-0.018; **Fig 4C**). This may explain the high correlation that we
298 observed between iGABA and the rates of GABA uptake estimated by radioactive
299 methods.

300 **3.4. GABA fluorescence may model haploinsufficiency of GAT-1 loss-of-function**
301 **variants in the context of wild-type GAT-1 co-expression**

302 As most variants reported in association with disease are monoallelic(Silva et al., 2024),
303 we next sought to assess the effects of combining WT with mutant hGAT1 variants in
304 the iGABA assay, mimicking the heterozygous state. We observed that the 1:1
305 combination of WT GAT-1 with pathogenic GAT-1 variants routinely increased
306 measured GABA uptake to a level ~50% 2xWT (**Fig 5A**). Meanwhile the benign I322M
307 variant with partially reduced iGABA increased to ~100% 2XWT (**Fig 5A**). Both findings
308 are expected for a simple additive effect and consistent with the putative disease
309 mechanism of haploinsufficiency. This also suggests that the transfection quantities
310 used for the assay were not saturating and that the read-out is in a linear range.

311 For two VUS associated with reduced GABA uptake (G111R, V511M) by the iGABA
312 method, we also observed an additive effect when combined with WT GAT-1 (**Fig 5A**).
313 However, for several VUS associated with only mild reductions in iGABA (L54F, R211C,
314 F242V, R419C, R566H, S574R), the addition of WT GAT-1 did not have the same
315 additive effect (6 of 6 VUS with reduced iGABA). This unexpected finding may suggest
316 an artifact of the heterologous system, but that is difficult to reconcile with the results
317 observed for pathogenic variants, the majority of which yielded evidence of an additive
318 effect (5 of 6 variants tested). Alternatively, these findings may suggest a disease
319 mechanism acting against the compensatory effects of WT GAT-1.

320 **3.5. GABA fluorescence provides insights into novel missense variant in GAT-1**

321 We used the iGABA assay to assess the effect of a novel missense variant in *SLC6A1*
322 in a patient with non-acquired focal epilepsy (NAFE).

323 Briefly, the proband was born at term with perinatal history complicated by intrauterine
324 drug exposure and planned repeat Cesarean section under general anesthesia. At
325 delivery, Apgar scores were 4 and 0 at one and five minutes, respectively, with
326 intubation in the delivery room and extubation to room air on day of life 1. He walked
327 independently by 15 months of age. However, language and social development were
328 delayed. He was diagnosed with autism spectrum disorder at 3 years old. At age 3
329 years, he spoke in word approximations and echolalia. He was quick to anger and

displayed head-banging and aggressive behavior. He made great progress in language and social development between the ages of 3.5-4 years in a preschool program for children with autism spectrum disorder. At 6 years old, he could participate in simple games, write and name some letters and numbers, cut with scissors, and use a brush to make paint strokes. He toilet-independently by 5 years old.

His seizure onset was at age 4 years, initially with semiology of staring with behavioral arrest, and he later developed seizures with left hemiclonic semiology. He has had 3 lifetime generalized tonic-clonic seizures. His seizure frequency increased over time and he experienced a developmental regression at 6 years old when seizures were poorly controlled. He lost the previously acquired language skills, interest in socializing, his behavior had worsened, and his gait became clumsy and somewhat crouched. At current age of 12 years, he has not regained the skills he lost despite improved seizure control. At last exam at 12 years old, he was able to speak in short sentences with quiet speech intermixed with jargoning and echolalia. His initial EEG showed right posterior temporal occipital epileptiform spikes. Subsequent EEGs at ages 6-9 years showed frequent sleep-potentiated multifocal spikes. At 11 years of age, an EEG showed runs of temporal-parietal focal spikes in sleep. He currently takes lamotrigine, which has been effective at seizure control. In the past, Prior regimens have included levetiracetam (stopped due to behavioral side effects), oxcarbazepine (ineffective), and valproic acid (the most effective but limited use due to side effect of thrombocytopenia). He also has a significant tremor in bilateral upper extremities that worsened with valproic acid but did not resolve after valproic acid was discontinued. He also continues to have tics, moderate intellectual disability, cortical visual impairment, behavioral problems attributed to ADHD and mood dysregulation, , as well as severe constipation. For his behavioral problems, which include impulsive behavior and aggression toward self and others, he has trialed multiple formulations of stimulant medications and antipsychotic medications. Behaviors have improved the most with guanfacine and valproic acid.

Radiological testing including MRI brain was unremarkable including no evidence of hypomyelination. He had unremarkable chromosomal microarray (CMA) and Fragile X testing. Whole-exome sequencing, updated in 2024, identified a variant in *SLC6A1*,

361 c.164 T>C (chr3-11059061; dbSNP, rs2124905468; GRCh38.p14 NC_000003.12, exon
362 3 of 16) resulting in p.M55T (Refseq, NM_003042.4). This variant is located in the 1st
363 transmembrane domain (**Fig 4A**), which is a recognized mutation hotspot(Silva et al.,
364 2024). It is predicted to be pathogenic by several pathogenicity prediction scores
365 (Revel, AlphaMissense, MUTAssessor, SIFT) though others classify it as benign
366 (PolyPhen2; MetaLR) (**Fig. 4B**). The variant is not present in the general population
367 (gnomAD) and is reported once in ClinVar as uncertain significance with limited clinical
368 description. Parental DNA was not available for segregation analysis as the patient was
369 adopted. Taken together, the patient's clinical presentation with seizures, tremor, and
370 intellectual disability was believed to be reasonably well-explained by the *SLC6A1*
371 p.M55T variant but with an ACMG classification of uncertain significance (criteria, PM2,
372 PP3).

373 The patient also harbored a heterozygous missense variant in GRIK2 c.1744G>A,
374 p.A582T (chr6-102337734; dbSNP, rs2484646253; GRCh38.p14, NM_021956.5, exon
375 12 of 17), which was not reported in ClinVar or other literature and was interpreted as
376 having uncertain significance. The VUS in GRIK2 was believed less likely to be a
377 primary cause of patient's epilepsy (criteria PM2, PP3) but cannot be fully excluded.
378 GRIK2 has recently been associated with neurodevelopmental disorders with DD and
379 prominent gait abnormalities(Stolz et al., 2021). The most severely affected patients (3
380 children with de novo variants at p.T660K and 2 children with p.T660R variants)
381 presented with global developmental delay, non-ambulatory status, onset of epilepsy
382 before age 3 years (4 out of 5 within 1st 12 mos), and brain MRI abnormalities in the first
383 years of life suggesting hypomelination, while the least severely affected patients (4
384 children and 1 adult with variants at p.A657T) presented with ID, DD, and
385 incoordination, but did not develop epilepsy and had normal MRIs(Stolz et al., 2021).
386 The reported variants cluster in two critical functional domains, the pore-forming M3
387 transmembrane helix and the adjacent M3-S2-gating linker(Stolz et al., 2021). In
388 contrast, our patient's GRIK2 variant (p.A582T) is not located in the implicated domains,
389 he developed seizures at age 4 yrs, ambulates, and has normal brain MRI, suggesting
390 poor overlap with known cases of GRIK2-associated NDD.

391 To understand the functional effects of the *SLC6A1* p.M55T variant, we assessed its
392 effects on GAT1-mediated GABA uptake using the iGABA assay (**Fig 4C.i**).
393 Surprisingly, the M55T variant is not associated with detectable reduction in GABA
394 uptake compared to WT controls (WT: 1 (mean) +/- 0.083 (sem), M55T: 1.11 +/- 0.102;
395 *p*=0.428, Welch's unpaired t-test; **Fig 4C.ii**), consistent with the PolyPhen2 prediction
396 (**Fig 4C.iii**). These findings may suggest limitations of GABA uptake assays in
397 heterologous cell lines, or they may suggest that the *SLC6A1* p.M55T variant does not
398 account for this patient's epilepsy.

399 **3.6. Assessment of iGABA reporter for drug responses and high-throughput**
400 **screening.**

401 We hypothesized that the iGABA-Snfr fluorescence assay of GAT-1 activity could be
402 suitable for screening compounds to identify new modulators of GABA transporter
403 activity.

404 To test this hypothesis, we developed a double stable cell line expressing both iGABA-
405 Snfr and hGAT1 constructs (Methods), and used the iGABA assay to assess the
406 response to the candidate compound, 4-phenylbutyric acid (4PBA) (**Fig 7A**). 4PBA was
407 previously described to have positive effects on GAT-1 through increased surface
408 expression of mutant and WT GAT-1(Nwosu et al., 2022). Given our previous findings
409 showing increased steady state iGABA in response to elevated hGAT1 dosage, the
410 correlation between rate of GABA uptake and steady state iGABA and the effect of
411 pathogenic variants on these parameters, we predicted that if 4PBA is therapeutically
412 effective, we should be able to detect its effect in our assay. Indeed, we observed a
413 significant ~35% increase in iGABA after treatment with 4PBA (1-3mM) in the setting of
414 GABA 1uM (vehicle: 0.434 (mean) +/- 0.006 (sem) fractional change in iGABA, vs
415 4PBA_1mM: 0.58 +/- 0.015, *p*= 0.0057; vs 4PBA_3mM: 0.595 +/- 0.020, *p*= 0.0023,
416 Dunnett's multiple comparison test) after 6 hour co-incubation (**Fig 7B**). These effects
417 were not significant at lower GABA (100nm). At higher GABA (10uM), the effect of
418 4PBA was equivocal, with lower concentration (4PBA_1mM; *p*= 0.0112) and a DMSO
419 control (*p*=0.0288) both significantly different from Vehicle1, but not higher
420 concentration (4PBA_3mM; *p*=0.195). This effect is not likely to be mediated by direct

421 interactions between 4PBA and the iGABA-Snfr sensor, as no increase in iGABA was
422 detected by direct *in vitro* testing (**Supplementary Fig 3**). These findings suggest that
423 the effect of 4PBA is detectable under specific assay conditions, despite differences
424 with previously reported assays(Nwosu et al., 2022), further corroborating its utility in
425 drug discovery.

426 We next evaluated the performance of the iGABA assay using the stable cell line in 384
427 well format using automated liquid handling devices and the high content fluorescence
428 imager (**Fig 8A**). To understand the sources of assay variance, we performed
429 preliminary testing with a 4-log range of GABA (10nM, 100nM, 1uM, 10uM) across
430 2x384 well plates, and fit covariates using a linear model (**Fig 8B.i**). We observed that
431 ~88.2% variance in iGABA was explained by this model (residual R^2, 0.1178), with the
432 GABA concentration accounting for the majority (71.4%, *p*=2.20E-16) followed by
433 intermediate contributions from the Column position (13.3%, *p*=2.20E-16), and minimal
434 contributions by Column*Order (1.3%, *p*=1.64E-15), Plate (1.1%, *p*=3.33E-13), Row
435 (0.7%, *p*=6.13E-09) and Row*Column (0.4%, *p*=8.52E-06). These findings suggested
436 that while GABA dose drives fluorescence largely independently of plate layout or minor
437 differences in incubation duration introduced by serial imaging, controlling these factors
438 would further improve assay performance.

439 We next compared the performance of adjusting iGABA using the background data
440 extracted from the linear model (LM) or an alternative linear mixed model (LMM)
441 incorporating random effects of well and plate (**Supplementary Fig 4A**). We observed
442 that the LMM adjustment better accounted for well-specific noise (**Supplementary Fig**
443 **4B**).

444 Next we assessed assay quality for the detection of positive modulators of GAT-1.
445 Given the weak effect of 4PBA and no confirmed positive agonist of GAT-1, we chose to
446 model the effects of strong positive modulation by utilizing 5X extracellular GABA (5 μM)
447 as positive control, which should significantly increase iGABA over the test condition
448 (GABA 1uM) based on preliminary data. Initial testing demonstrated that the assay
449 quality index β (derived from robust strictly standardized mean difference (RSSMD)
450 positive vs negative control) was in the *moderate* range (median, 2.91) using raw

451 iGABA and in the *strong* range (median, 4.3) using adjusted iGABA following plate
452 normalization with fixed and random effects from LMM (**Fig 8C**).

453 To identify the optimal number of control replicates for desired assay performance, we
454 performed bootstrap stimulations for a single concentration primary screen without
455 replicates versus a variable number of on-plate control replicates (4 to 24) for negative
456 (GABA1uM) and positive (GABA 5uM) controls. We observed that a primary screen
457 without replicates could detect significant increases in iGABA above background with a
458 minimum RSSMD threshold = 2.2, assuming 10 negative control replicates. With raw
459 iGABA, the positive control RSSMD threshold was 2.43, assuming 10 positive control
460 replicates, suggesting a narrow window above background to detect compounds whose
461 effect size is less than positive control or to prioritize compounds by their relative effect
462 sizes. However with adjusted iGABA, the positive control RSSMD threshold was 4.94,
463 yielding a larger window for detection and prioritization. This performance window
464 continues to improve with additional replicates using either approach such that with 24
465 replicates each (positive and negative) the raw iGABA approach has a minimum
466 RSSMD threshold = 1.86 and positive control RSSMD = 2.69, while adjusted iGABA
467 has thresholds 1.90 and 5.85, respectively. These findings suggest the double stable
468 iGABA-Snfr hGAT1 cell line may be suitable for high-throughput compound screening,
469 and that the use of a linear mixed model for plate normalization may improve the
470 prioritization of active compounds.

471 **4. Discussion**

472 For patients with epilepsy undergoing genetic testing, identification of a variant in a
473 gene related to epilepsy is generally not sufficient to make a diagnosis, and relies in part
474 on functional assays of gene function. Although mature assays exist for proteins like
475 GAT-1 encoded by *SLC6A1*, the use of radioactivity limits ease of adoption or its
476 application to compound screening. Although recent reports provide extensive
477 functional predictions for over 200 human variants in *SLC6A1*(Silva et al., 2024), there
478 continue to be new human variants needing functional interrogation. Towards those
479 ends, we developed a non-radioactive cell-based assay for functional validation of
480 human GAT-1 coding sequence variants and compound screening using a previously

481 described genetically-encoded GABA fluorescence sensor (iGABA-Snfr) and high-
482 throughput automated microscopy.

483 **4.1. Validation of the iGABA assay of GAT-1 function**

484 We established that variant-specific iGABA is highly correlated with GABA uptake
485 estimates from radioactive assays(Silva et al., 2024), and validated the assay's ability to
486 detect reduced GABA uptake in pathogenic variants and re-classify VUS as pathologic
487 based on reduced iGABA. As predicted, the results of specific GAT-1 variants on the
488 iGABA assay are largely similar to those of [3H]-GABA uptake. Using a conservative
489 pathogenic threshold based on the lower limit (95th CI) of pathogenic variants tested, ,
490 we demonstrated pathogenic loss-of-function (LoF) in 3 VUS (G111R, S459R, and
491 V511M), corroborating a recent report that showed severe LoF in two (G111R, S495R)
492 and intermediate LoF in another (V511M)(Silva et al., 2024). Meanwhile, 6 additional
493 VUS showed reductions that did not meet our pathogenic threshold (L54F, S574R,
494 F242V, R211C, R419C, and R566H). Based on [3H]-GABA assays, half of these have
495 been previously associated with "typical" GABA uptake (S574R, F242V, R419C),
496 whereas the remaining half have been associated with intermediate LoF (L54F, R211C,
497 and R566H)(Silva et al., 2024). We believe the differences in this case are due to the
498 use of multiple thresholds by other authors, but not due to major discrepancies in the
499 estimated GABA uptake. Together, these observations suggest excellent agreement
500 with prior reports.

501 We also assessed iGABA as a function of time in a pathogenic variant with residual
502 GABA uptake (V342M) and showed how lower rates of GABA transport are correlated
503 with lower variant-specific steady-state iGABA. Specifically, the change in rate (at least
504 in the case of the V342M variant) can be accounted for mathematically merely by the
505 shift in steady state. This relationship did not have to hold true, as GAT-1 variant-
506 mediated reductions in rate of GABA uptake could in theory reach the same steady
507 state on longer time-scales. However, this does not appear to be the case under these
508 assay conditions (6 hrs), which are likely an overly generous incubation interval
509 compared to the dynamic *in vivo* extracellular environment. Future investigations may

510 explore the extent that this relationship holds true for other patient-derived GAT-1
511 variants.

512 **4.2. Unexpected interactions between WT and mutant GAT-1 variants with**
513 **residual GABA uptake**

514 We also showed how iGABA responds to the combination of WT with mutant GAT-1,
515 mimicking the heterozygous state that is typical for *SLC6A1*-related disorders. The
516 studies showed the expected additive boost in GAT-1 activity when WT GAT-1 was
517 combined with known pathogenic variants or with VUS with significantly reduced GABA
518 uptake activity (assessed by iGABA), but unexpectedly did not show an additive effect
519 when combined with variants possessing substantial residual GABA uptake activity. It
520 does not appear to be explained by the dynamic range of the assay, given the results
521 from the benign I322M variant. This may suggest a dominant negative effect acting
522 against the compensatory effects of WT GAT-1 supplied *in trans.*

523 A potential dominant negative (DN) mechanism of SLC6A1-related disease has been
524 raised several times (Carvill et al., 2015; Johannesen et al., 2018; Silva et al., 2024), but
525 to our knowledge most reports to date have been largely consistent with
526 haploinsufficiency. Few reports have convincingly demonstrated a negative interaction
527 between hypomorphic GAT-1 variants and WT GAT-1 function, though relevant data
528 has been reported for only a limited number of variants. Most similar to our own assay,
529 Silva et al. examined combined WT GAT-1 with equimolar variant DNA, including two
530 variants with typical GABA uptake (Asp43Glu, Ile434Met) and five severe LoF variants
531 (Gly63Ser, Tyr140Cys, Ser295L, Leu547Arg, Gly550R), and reported no evidence of
532 DN(Silva et al., 2024). Similar to our data, the authors showed additive increases for
533 variants with severe LoF. However, the authors' control data suggests that their assay
534 read-out was not in a linear range between 1XWT to 2XWT, making precise
535 interpretation of the results of the variants with typical GABA uptake less clear. Nwosu
536 et al examined a series of GAT-1 variants by [3H]-GABA uptake assay in HEK293T
537 cells with or without 1:1 combinations with WT GAT-1 in the setting of 4PBA
538 treatment(Nwosu et al., 2022), but their method of normalization prevents easy
539 comparison with the results of our study.

540 Based on *in vivo* studies, the Kang group has stated that the epileptic phenotype of
541 S295L and A288V may be more severe than *SLC6A1* knock-out heterozygotes (Shen et
542 al., 2024), suggesting dominant negativity, but the basis for this interpretation is not
543 clear. By contrast, Lindquist et al(Lindquist et al., 2023) showed similar rates of spike-
544 wave discharges (SWDs) and behavioral arrest in *Slc6a1*-S295L/+ mice compared to a
545 *Slc6a1 +/-* knock-out, though the mouse strains were different (C57BL/6 vs hybrid
546 C57BL/6.129S1, respectively) which may confound a quantitative comparison.
547 Separately, Shen et al(Shen et al., 2024) reported differences in residual GABA uptake
548 between heterozygous and homozygous mice of the S295L and A288V lines, with
549 similar reductions noted between hets (~42-51% vs WT), but with greater residual
550 activity (~30% WT) in A288V/A288V vs S295L/S295L (~0% WT). This effect is similar to
551 the non-additive effect we observe *in vitro* for other variants, though notably not for the
552 A288V which had virtually no GABA uptake activity in our assay.

553 Ultimately, we anticipate that it will be important to investigate the potential dominant
554 negative functions of mutant GAT-1 further, as it may have a significant impact on
555 methods of variant interpretation. Although the clinical evidence available suggests a
556 strong correlation between variants with severe LoF in GABA uptake and severe
557 epilepsy phenotypes (e.g. EMAS, EOAE, DEE) (Silva et al., 2024), it has not yet been
558 rigorously established how to interpret variants whose GABA uptake is assessed as
559 falling within a conservative “typical” range (e.g. -49.2% to +47.5% in Silva et al.), which
560 appears to comprise ~40% of all reported variants. Indeed, although none of the
561 variants in this experiment exceeded our pathogenic threshold (-71.5% reduction vs
562 WT) under “homozygous” conditions, after being combined with WT GAT-1, all of these
563 variants demonstrate GABA uptake similar to that of pathogenic variants combined with
564 WT. This observation raises questions regarding the most appropriate conditions for
565 defining the pathogenicity of mild GAT-1 variants.

566 Future work should examine the basis for this apparent negative interaction with WT
567 GAT-1 in the “heterozygous” setting, and whether it better correlates with *in vivo* assays
568 of GABA uptake and clinical severity especially for variants with mild loss-of-function.

569 **4.3. Case report highlights limitations of GABA uptake assays**

570 We also report the case summary of a boy with NAFE whose M55T variant in *SLC6A1*
571 is associated with normal GABA uptake by the iGABA assay. This variant has been
572 reported once (ClinVar 1307517) but with limited information regarding associated
573 clinical findings or inheritance, and its effects on GABA uptake have not been previously
574 reported. We are confident in our assessment of GABA uptake, given the high
575 correlation between prior radioactive studies and the iGABA assay, as well as the fact
576 that the level of GABA transport activity associated with M55T is indistinguishable from
577 WT, while being higher than any of the pathogenic or VUS variants we studied (15 total,
578 including M55T). This suggests that the M55T variant does not alter GABA transport
579 under these conditions, but we cannot exclude the possibility for different effects under
580 different assay conditions (as discussed in **Section 4.2**), or *in vivo*, nor can we exclude
581 its involvement in other less well-characterized mechanisms that may contribute to
582 *SLC6A1* haploinsufficiency. At the same time, we do not believe that the co-occurring
583 VUS in *GRIK2* is a better explanation, as the patient's case is not clinically consistent
584 with what is currently known regarding *GRIK2*-associated NDD or epilepsy (see
585 **Section 3.5**). Together, his case highlights the challenge of establishing genetic
586 diagnoses when limited functional evidence is available.

587 For additional context, we wondered how often clinically ascertained missense variants
588 in *SLC6A1* are not associated with changes in GABA uptake. Based on the most
589 comprehensive analysis of clinically ascertained GAT-1 variants published to date(Silva
590 et al., 2024)(which did not evaluate M55T), there are 28 variants (out of 192 analyzed,
591 ~14.6%) whose [3H]-GABA transporter activity was unchanged or hyperfunctioning,
592 suggesting it is not a rare phenomenon. Half (14 out of 28) were reported in association
593 with epilepsy. Many of these variants are observed in the general population (gnomAD)
594 and their inheritance patterns not reported, reducing confidence in a causal association.
595 However, at least one nearby variant also located in TM1a, p.F51Y, is not present in
596 population databases, has conflicting interpretations in ClinVar (1 benign, and 1
597 uncertain), and has been reported to have normal GABA uptake and surface expression
598 (Silva et al., 2024).

599 Similarly, Silva et al. reported that across epilepsy types, variants reported in
600 association with NAFE (as in our patient) showed GABA uptake that was exclusively in

601 the “typical” or unaffected range. In contrast, variants associated with EMAS were
602 predominantly severe LoF. Although Silva et al. concluded that *SLC6A1* may therefore
603 not be associated with NAFE, this phenomenon could also suggest limitations of
604 heterologous cell lines or assay conditions to recapitulate disease-relevant functions of
605 GAT-1, particularly for variants with mild or no effects on GABA uptake. Ultimately, the
606 pathogenicity of this class of variants warrants further investigation, ideally in animal
607 models where comprehensive evaluations in an intact biological system are possible.

608 **4.4 Drug screening.**

609 Last we demonstrated the suitability of iGABA for compound screening to identify novel
610 positive modulators of GAT-1. We showed how 4PBA -- a molecular chaperone which
611 appears to increase GAT-1-mediated GABA transport *in vitro* and in preclinical mouse
612 models(Nwosu et al., 2022) – has a mild effect in our assay at specific concentrations of
613 extracellular GABA (1uM). We believe this is largely consistent with the magnitude of
614 effect reported in the literature (~1.2-1.4x increase), accounting for differences in
615 reported assay conditions(Nwosu et al., 2022). Although 4PBA may show clinical
616 promise, the availability of a high-throughput image-based assay of GAT-1 function may
617 facilitate the identification of more specific positive modulators of GAT-1.

618 **4.5 Advantages and limitations of iGABA**

619 Overall, the iGABA assay has the advantages of lower cost and regulatory restrictions
620 compared to radioactive assays, it is portable to any lab with fluorescence microscopy
621 and can be adapted to any high-throughput workflow using automated imaging. We
622 anticipate iGABA will be sensitive to a broad domain of therapeutic agents, including
623 agents that affect uptake rate, surface expression, and intracellular GABA retention, all
624 of which may be biologically relevant for GABA regulation.

625 We also acknowledge limitations in the iGABA assay. First, the assay measures steady-
626 state intracellular GABA at a single timepoint, not the rate of GABA uptake, making it
627 less sensitive at short incubation durations compared to radioactive uptake, and
628 possibly confounded by other processes affecting the intracellular accumulation of
629 GABA (such as GABA metabolism, sequestration or release). Nevertheless, PAMs
630 enhancing steady-state levels would likely translate to increased GABA clearance *in*

631 *vivo*, a therapeutic goal for SLC6A1-related disorders like epilepsy. Second, as
632 previously reported(Marvin et al., 2019), compounds with structural similarity to GABA
633 may be a source of false positives in the context of drug screening with iGABA-Snfr,
634 necessitating confirmation of active compounds by orthogonal assays. Third, as
635 discussed, heterologous cell lines may not recapitulate neural-specific modes of GAT-1
636 regulation and function. Fourth, the described method is limited to coding variants but
637 could be easily extended to assess effects of non-coding or splicing related variants in
638 patient-derived cells, as reported for [3H]-GABA assays(Nwosu et al., 2022).

639 **5. Conclusion**

640 In summary, the non-radioactive iGABA assay appears suitable for functional validation
641 of GAT-1 variants as well as high-throughput compound screening to identify positive
642 modulators of GAT-1.

643 **6. Data and reagent availability statement.** All of the data generated in the present
644 study are available upon request. Plasmids from this study (V006-2, V007-2.2) will be
645 deposited in AddGene. The hGAT1-iGABA cell line is available upon request.

646 **7. Acknowledgements.**

647 We thank Lee Barrett for technical assistance. This work made use of resources
648 through the F.M. Kirby Assay Development and Screening Facility (ADSF) at Boston
649 Children's Hospital. We thank Amber Freed (SLC6A1 Connect), Michael Kavanaugh
650 (University of Montana) and Henry Lee (BCH) for helpful discussions, and Jonathan
651 Marvin (Janelia) for providing the data regarding the direct effects of 4PBA on iGABA-
652 Snfr fluorescence.

653 **8. Author contributions using the CRediT taxonomy.**

654 CM: Conceptualization, Data curation, Formal analysis, Funding acquisition,
655 Investigation, Methodology, Software, Visualization, Supervision, Writing – original draft,
656 Writing – review and editing. GZ: Investigation. GP: Investigation. KW: Writing – review
657 and editing. AP: Funding acquisition, Supervision, Writing – review and editing.

658 **9. Funding information.** CMM was supported by NIH / NINDS K08NS118107. AP was
659 supported by the Diamond Blackfan Chair in Neuroscience Research and the Robinson
660 Fund for Transformative Research in Epilepsy.

661 **10. Competing interests.** The authors have no competing interests to declare. Dr.
662 Poduri was an employee of the National Institutes of Health during the initial drafting of
663 this manuscript. This report does not represent the official view of NIH or any part of the
664 U.S. Federal Government. No official support or endorsement of this article by the
665 NINDS or NIH is intended or should be inferred.

666 **11. Figure captions**

667 **Figure 1. Development of a cell-based assay for hGAT-1 function using iGABA-**
668 **Snfr fluorescence.** (**A**) Schematic of constructs (pCDNA3.1) used to express human
669 GAT-1 (*upper*) and a genetically encoded GABA sensor, iGABA-Snfr (*lower*) with
670 stoichiometrically linked fluorophores. Not to scale. (**B**) Approach to quantifying GAT-1-
671 mediated GABA uptake in HeLa cells. In the presence of exogenous GABA and GAT-1
672 protein, elevated intracellular concentration of GABA ($[GABA]_i$) is reflected by increased
673 fluorescence by iGABA-Snfr. (**C**) Workflow for assays to validate the function of GAT-1
674 variants and the detection of agonist compounds. (**D**) Representative images of iGABA
675 assay and mock-up of automated analysis to measure per-cell average iGABA-Snfr
676 fluorescence. Scale bar = 50 um. (**E**) Relative frequency histograms of iGABA-Snfr
677 fluorescence after incubation with GABA (100uM) versus vehicle (DMSO), as measured
678 by automated analysis at the per-cell level within a single site (*top*) and the per-well
679 averages (*lower*) across a representative 96-well plate (N=48 wells per condition, 4 sites
680 per well).
681

682 **Figure 2. Validation of iGABA-Snfr assay for assessing GAT-1 loss-of-function**
683 **variants.**
684 (**A**) Schematic of full-length human GAT-1 protein (Uniprot P30531) and the
685 location/range of deletions implicated in ΔCPD (cytoplasmic domain), ΔECD
686 (extracellular domain), and ΔTM6-7 (transmembrane domains 6 and 7). (**B**) GABA
687 concentration series (5-log range) demonstrates enhanced intracellular GABA
688 accumulation in wildtype GAT-1 compared to GAT-1 constructs harboring deletions of
689 critical domains (ECD, CPD, and TM6-7). (Two-way ANOVA, with Dunnett's multiple
690 comparisons test; 6 families, 3 comparisons per family, relative to WT). (**C-D**)
691 Normalized change in iGABA fluorescence (C) and as %WT (D) is significantly greater

692 in wildtype GAT-1 versus GAT-1 deletion constructs at GABA concentrations 1uM-
693 100uM. For each construct, data are the difference in iGABA fluorescence between
694 GABA conditions and vehicle control, divided by vehicle control. (Two-way ANOVA, with
695 Dunnett's multiple comparisons test; 3 families, 3 comparisons per family, relative to
696 WT). (**E**) The robust strictly standardized mean difference (RSSMD) and robust z-prime
697 are calculated between positive (GABA 1uM) and negative (vehicle) controls (*right*)
698 across replicate plates. For B-D, assay format is 96-well plate, transient transfection,
699 incubation time 6-7 hrs. Data are the mean +/- SEM of independent per-well averages
700 of iGABA (4 wells per condition (construct x GABA concentration), 4 sites per well)
701

702 **Figure 3. Validation of iGABA-Snfr assay for assessing human GAT-1 variants.**
703 (**A)** Schematic of human GAT-1 protein (Uniprot P30531) and human variants tested in
704 this study. Boxes indicate the amino acid substitution associated with each missense
705 variant. Color coding indicates clinical classification based on ClinVar. (**B)**
706 Representative results of iGABA assay as a function of variant. Data are fractional
707 changes in GABA fluorescence expressed as mean +/- sem in the presence of GABA
708 1uM relative to untreated control for each construct (4 wells per condition). (**C)**
709 Significant impairments in fractional iGABA change is noted in all pathogenic variants
710 tested and a subset of VUS. Data are mean +/- sem for grouped variants shown in B.
711 (n=4 wells per condition). Kruskal-Wallis test with Dunnett's test; **, p*<0.05. (**D)** iGABA
712 test-retest correlation for GAT-1 variants is high (R^2=0.8498). Data are fractional GABA
713 uptake relative to WT control from two independent experiments (n=4 wells per
714 condition). (**E**) Variant-specific GABA fluorescence is closely correlated (R^2=0.8095)
715 with published 3H-GABA uptake assays. Data is adapted from the "UCSF dataset"
716 published by Silva et al AJHG 2024 (https://doi.org/10.1016/j.ajhg.2024.04.02). (**F)**
717 Significant correlations between fractional iGABA and PolyPhen2 (i) and AlphaMissense
718 (ii) scores
719

720 **Figure 4. Pathogenic variants in GAT-1 are associated with reduced steady-state**
721 **iGABA.** (**A**) Time-course experiments following 1-6 hours incubation demonstrate

722 marked reduction in plateau of $[GABA]_{in}$ mediated by mutant GAT-1 V342M versus GAT-
723 1 WT control. Data are average +/- s.e.m. (n=15 wells per timepoint x condition). Non-
724 linear fits were computed based on pseudo-first order association kinetics, according to
725 the equation `Y=Y0 + (Plateau-Y0)*(1-exp(-K*x))`. Statistics are unpaired t-test
726 with Welch correction with FDR correction. ****, adjusted p<0.0001. (**B-C**) Parameters
727 from non-linear fit of (A) shows significantly reduced steady-state levels (parameter
728 Plateau; B) but no significant difference in the rate constant (parameter K; C). Data are
729 best-fit parameter values +/- 95% C.I.
730

731 **Figure 5. Complex variant-dependent interactions between WT and mutant GAT-1**
732 **affect GABA uptake.** (**A-B**) Effects of combining GAT-1 variants with equimolar WT
733 GAT-1 by transient transfection show additive (A) and non-additive (B) effects. Data are
734 fractional change in iGABA relative to control (4 wells per condition), presented as mean
735 +/- sem. The MUT series (*open boxes*) are normalized by WT, while MUT+WT data
736 (*checkerboard*) are normalized by 2xWT. Statistics are Dunnett's test for differences
737 between MUT vs MUT+WT for each variant followed by false-discovery rate (FDR)
738 correction (n.s., not significant. *, *adj p*<0.05. **, *adj p*<0.01. ***, *adj p*<0.001).
739

740 **Figure 6. iGABA assay can evaluate functional effects of novel coding sequence**
741 **variants on GABA transport. (A)** The p.M55T variant is located within the 1st
742 transmembrane (TM) domain of GAT-1 (Uniprot P30531). Sanger sequencing of the
743 GAT-1 p.M55T construct used in iGABA assay is shown. (**B)** Pathogenicity prediction
744 scores for p.M55T are equivocal, with several suggesting deleterious effect but others
745 not (PolyPhen2, MetaLR). (**C**) Approach to assay the effects of novel human GAT-1
746 variants on iGABA (i) and its negligible effects on GABA uptake (ii), in good
747 correspondence with PolyPhen2 score (iii). Data are mean +/- sem, expressed relative
748 to WT controls (n=15 wells per condition; 6 sites per well). Statistics are unpaired T-test
749 with Welch's correction. n.s., not significant.
750

751 **Figure 7. Mild effect of 4-phenylbutyric acid (4PBA) on GAT-1 activity in iGABA**
752 **assay.**
753 (**A**) Structure of 4-phenylbutyric acid, 4PBA (i) and schematic for experiment (ii). (**B**)
754 Mild enhancement of iGABA by 4PBA following application of GABA (0.1-10uM). Data
755 are mean +/- sem. (n=4 wells per condition; 96-well format; 6 hour incubation). Controls
756 include two duplicate vehicle controls (H2O; Vehicle1-2), and a DMSO (0.05%) control.
757 Statistics are one-way ANOVA followed by Dunnett's multiple comparison relative to
758 control ("Vehicle 1"). n.s., not significant. *, $p<0.05$, **, $p<0.01$, ***, $p<0.001$.
759

760 **Figure 8. Validation of high-throughput screening strategy to identify GAT-1**
761 **agonists using iGABA fluorescence in live cells.** (**A**) Proposed work-flow for high-
762 throughput screening includes: 1) stable HeLa cell line expressing iGABA-Snfr and
763 hGAT-1 in 384-well format; 2) application of GABA + test compounds using automated
764 liquid handler (Bravo). The GABA concentration for screening is 1uM, given highly
765 specific GAT-1-dependent uptake at this range. As there are no known GAT-1 agonists,
766 a higher concentration of GABA (5uM) is used as a positive control. Incubation duration
767 = 6-8 hrs; 3) measurement of iGABA fluorescence using automated high-content
768 imaging (IXM); 4) plate normalization and quality control; 5) hit detection and
769 prioritization based on robust strictly standardized mean difference (RSSMD). In a
770 primary screen, compounds whose RSSMD versus on-plate negative controls (GABA
771 1uM) exceed the $RSSMD_{FPR \leq 5\%}$ threshold are considered hits; compounds whose
772 RSSMD exceed the $RSSMD_{TPR \geq 95\%}$ threshold have effect size similar to positive
773 control. (**B**) A linear model (i) estimates the variance in iGABA explained by covariates
774 (ii). Data are barplots of model R^2 or residual R^2 values calculated from ANOVA, and
775 written beside each bar . Statistics are F-tests from ANOVA. ***, $p<0.001$. (**C**) Assay
776 quality based on RSSMD between positive control (GABA 5uM) and negative control
777 (GABA 1uM) for raw iGABA (*left*) and adjusted iGABA (*right*) following plate
778 normalization. Data are RSSMD of iGABA fluorescence (n=28 wells per replicate x
779 condition) from 2 plates, each with 2 replicas (=4 replicates). (**D-E**) Bootstrap
780 simulations from raw iGABA (D) and adjusted iGABA (E) to identify RSSMD screening
781 thesholds for a primary screen without replicates. Thresholds are shown as functions of

782 the number of on-plate replicate controls versus a single test well. The threshold for hit
783 detection (*blue*) maintains FPR≤5%, while the threshold for detecting compounds with
784 effects as large as positive control (GABA 5uM; *red*) maintains TPR≥95%. Vertical
785 dotted lines indicate the RSSMD thresholds @ N=10 replicates . See Method section for
786 further details.
787
788 **12. Table 1.** Clinical and molecular characterization of GAT-1 variants investigated in
789 this study.
790
791 **13. Supplementary material**
792 Supplementary Figure 1-4 and captions.
793 Supplementary Table 1.
794
795 **14. References.**
796 Cai, K., Wang, J., Eissman, J., Wang, J., Nwosu, G., Shen, W., Liang, H.-C., Li, X.-J., Zhu, H.-
797 X., Yi, Y.-H., Song, J., Xu, D., Delpire, E., Liao, W.-P., Shi, Y.-W., & Kang, J.-Q. (2019).
798 A missense mutation in SLC6A1 associated with Lennox-Gastaut syndrome impairs
799 GABA transporter 1 protein trafficking and function. *Experimental Neurology*, *320*,
800 112973. https://doi.org/10.1016/j.expneurol.2019.112973
801 Carvill, G. L., McMahon, J. M., Schneider, A., Zemel, M., Myers, C. T., Saykally, J., Nguyen, J.,
802 Robbiano, A., Zara, F., Specchio, N., Mecarelli, O., Smith, R. L., Leventer, R. J., Møller,
803 R. S., Nikanorova, M., Dimova, P., Jordanova, A., Petrou, S., Helbig, I., … Mefford, H. C.
804 (2015). Mutations in the GABA Transporter SLC6A1 Cause Epilepsy with Myoclonic-
805 Atonic Seizures. *The American Journal of Human Genetics*, *96*(5), 808–815.
806 https://doi.org/10.1016/j.ajhg.2015.02.016

807 Eglen, R. M., & Reisine, T. (2009). New Insights into GPCR Function: Implications for HTS. In
808 W. R. Leifert (Ed.), *G Protein-Coupled Receptors in Drug Discovery* (pp. 1–13). Humana
809 Press. https://doi.org/10.1007/978-1-60327-317-6_1
810 Johannesen, K. M., Gardella, E., Linnankivi, T., Courage, C., Saint Martin, A., Lehesjoki, A.-E.,
811 Mignot, C., Afenjar, A., Lesca, G., Abi-Warde, M.-T., Chelly, J., Piton, A., Merritt, J. L.,
812 Rodan, L. H., Tan, W.-H., Bird, L. M., Nespeca, M., Gleeson, J. G., Yoo, Y., … Møller, R.
813 S. (2018). Defining the phenotypic spectrum of SLC6A1 mutations. *Epilepsia*, *59*(2),
814 389–402. https://doi.org/10.1111/epi.13986
815 Lindquist, B. E., Voskobiynyk, Y., Goodspeed, K., & Paz, J. T. (2023). Patient-derived SLC6A1
816 variant S295L results in an epileptic phenotype similar to haploinsufficient mice.
817 *Epilepsia*, *64*(10), e214–e221. https://doi.org/10.1111/epi.17731
818 Marvin, J. S., Shimoda, Y., Magloire, V., Leite, M., Kawashima, T., Jensen, T. P., Kolb, I., Knott,
819 E. L., Novak, O., Podgorski, K., Leidenheimer, N. J., Rusakov, D. A., Ahrens, M. B.,
820 Kullmann, D. M., & Looger, L. L. (2019). A genetically encoded fluorescent sensor for in
821 vivo imaging of GABA. *Nature Methods*, *16*(8), 763–770. https://doi.org/10.1038/s41592-
822 019-0471-2
823 Mattison, K. A., Butler, K. M., Inglis, G. A. S., Dayan, O., Boussidan, H., Bhambhani, V.,
824 Philbrook, B., Silva, C., Alexander, J. J., Kanner, B. I., & Escayg, A. (2018). SLC6A1
825 variants identified in epilepsy patients reduce γ-aminobutyric acid transport. *Epilepsia*,
826 *59*(9), e135–e141. https://doi.org/10.1111/epi.14531
827 Nwosu, G., Mermer, F., Flamm, C., Poliquin, S., Shen, W., Rigsby, K., & Kang, J. Q. (2022). 4-
828 Phenylbutyrate restored γ-aminobutyric acid uptake and reduced seizures in SLC6A1
829 patient variant-bearing cell and mouse models. *Brain Communications*, *4*(3), fcac144.
830 https://doi.org/10.1093/braincomms/fcac144
831 Rees, E., Han, J., Morgan, J., Carrera, N., Escott-Price, V., Pocklington, A. J., Duffield, M., Hall,
832 L. S., Legge, S. E., Pardiñas, A. F., Richards, A. L., Roth, J., Lezheiko, T., Kondratyev,

833 N., Kaleda, V., Golimbet, V., Parellada, M., González-Peñas, J., … Owen, M. J. (2020).
834 De novo mutations identified by exome sequencing implicate rare missense variants in
835 SLC6A1 in schizophrenia. *Nature Neuroscience*, *23*(2), 179–184.
836 https://doi.org/10.1038/s41593-019-0565-2
837 Richerson, G. B., & Wu, Y. (2004). Role of the GABA Transporter in Epilepsy. In D. K. Binder &
838 H. E. Scharfman (Eds.), *Recent Advances in Epilepsy Research* (Vol. 548, pp. 76–91).
839 Springer US. https://doi.org/10.1007/978-1-4757-6376-8_6
840 Shen, W., Nwosu, G., Honer, M., Clasadonte, J., Schmalzbauer, S., Biven, M., Langer, K.,
841 Flamm, C., Poliquin, S., Mermer, F., Dedeurwaerdere, S., Hernandez, M.-C., & Kang, J.-
842 Q. (2024). γ-Aminobutyric acid transporter and GABAA receptor mechanisms in
843 Slc6a1+/A288V and Slc6a1+/S295L mice associated with developmental and epileptic
844 encephalopathies. *Brain Communications*, *6*(2), fcae110.
845 https://doi.org/10.1093/braincomms/fcae110
846 Silva, D. B., Trinidad, M., Ljungdahl, A., Revalde, J. L., Berguig, G. Y., Wallace, W., Patrick, C.
847 S., Bomba, L., Arkin, M., Dong, S., Estrada, K., Hutchinson, K., LeBowitz, J. H.,
848 Schlessinger, A., Johannesen, K. M., Møller, R. S., Giacomini, K. M., Froelich, S.,
849 Sanders, S. J., & Wuster, A. (2024). Haploinsufficiency underlies the
850 neurodevelopmental consequences of SLC6A1 variants. *The American Journal of*
851 *Human Genetics*, *111*(6), 1222–1238. https://doi.org/10.1016/j.ajhg.2024.04.021
852 Stolz, J. R., Foote, K. M., Veenstra-Knol, H. E., Pfundt, R., ten Broeke, S. W., de Leeuw, N.,
853 Roht, L., Pajusalu, S., Part, R., Rebane, I., Õunap, K., Stark, Z., Kirk, E. P., Lawson, J.
854 A., Lunke, S., Christodoulou, J., Louie, R. J., Rogers, R. C., Davis, J. M., … Swanson,
855 G. T. (2021). Clustered mutations in the GRIK2 kainate receptor subunit gene underlie
856 diverse neurodevelopmental disorders. *American Journal of Human Genetics*, *108*(9),
857 1692–1709. https://doi.org/10.1016/j.ajhg.2021.07.007

858 Wu, Y., Wang, W., Díez-Sampedro, A., & Richerson, G. B. (2007). Nonvesicular inhibitory
859 neurotransmission via reversal of the GABA transporter GAT-1. *Neuron*, *56*(5), 851–865.
860 https://doi.org/10.1016/j.neuron.2007.10.021
861 Zhang, X. D. (2011). Illustration of SSMD, z score, SSMD*, z* score, and t statistic for hit
862 selection in RNAi high-throughput screens. *Journal of Biomolecular Screening*, *16*(7),
863 775–785. https://doi.org/10.1177/1087057111405851
864

Figure 1

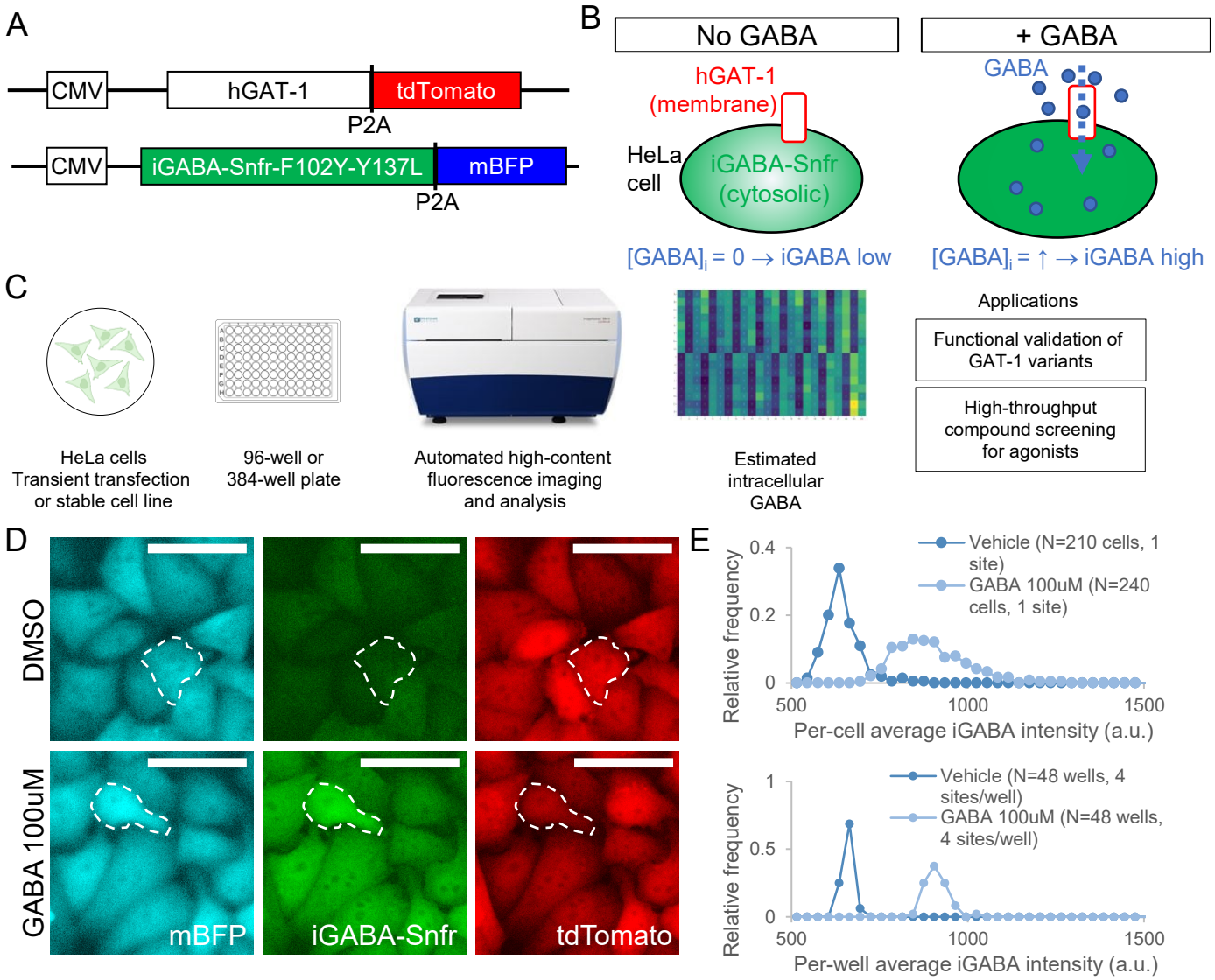
A
CMV
hGAT-1
tdTomato
P2A
CMV
iGABA-Snfr-F102Y-Y137L
mBFP
P2A
B
No GABA
+ GABA
hGAT-1
(membrane)
HeLa
cell
iGABA-Snfr
(cytosolic)
GABA
[GABA]i = 0 → iGABA low
[GABA]i = ↑ → iGABA high
C
HeLa cells
Transient transfection
or stable cell line
96-well or
384-well plate
Automated high-content
fluorescence imaging
and analysis
Estimated
intracellular
GABA
Applications
Functional validation of
GAT-1 variants
High-throughput
compound screening
for agonists
D
DMSO
GABA 100uM
mBFP
iGABA-Snfr
tdTomato
E
Vehicle (N=210 cells, 1 site)
GABA 100uM (N=240 cells, 1 site)
Relative frequency
0.4
0.2
0
500
1000
1500
Per-cell average iGABA intensity (a.u.)
Vehicle (N=48 wells, 4 sites/well)
GABA 100uM (N=48 wells, 4 sites/well)
Relative frequency
1
0.5
0
500
1000
1500
Per-well average iGABA intensity (a.u.)

Figure 2

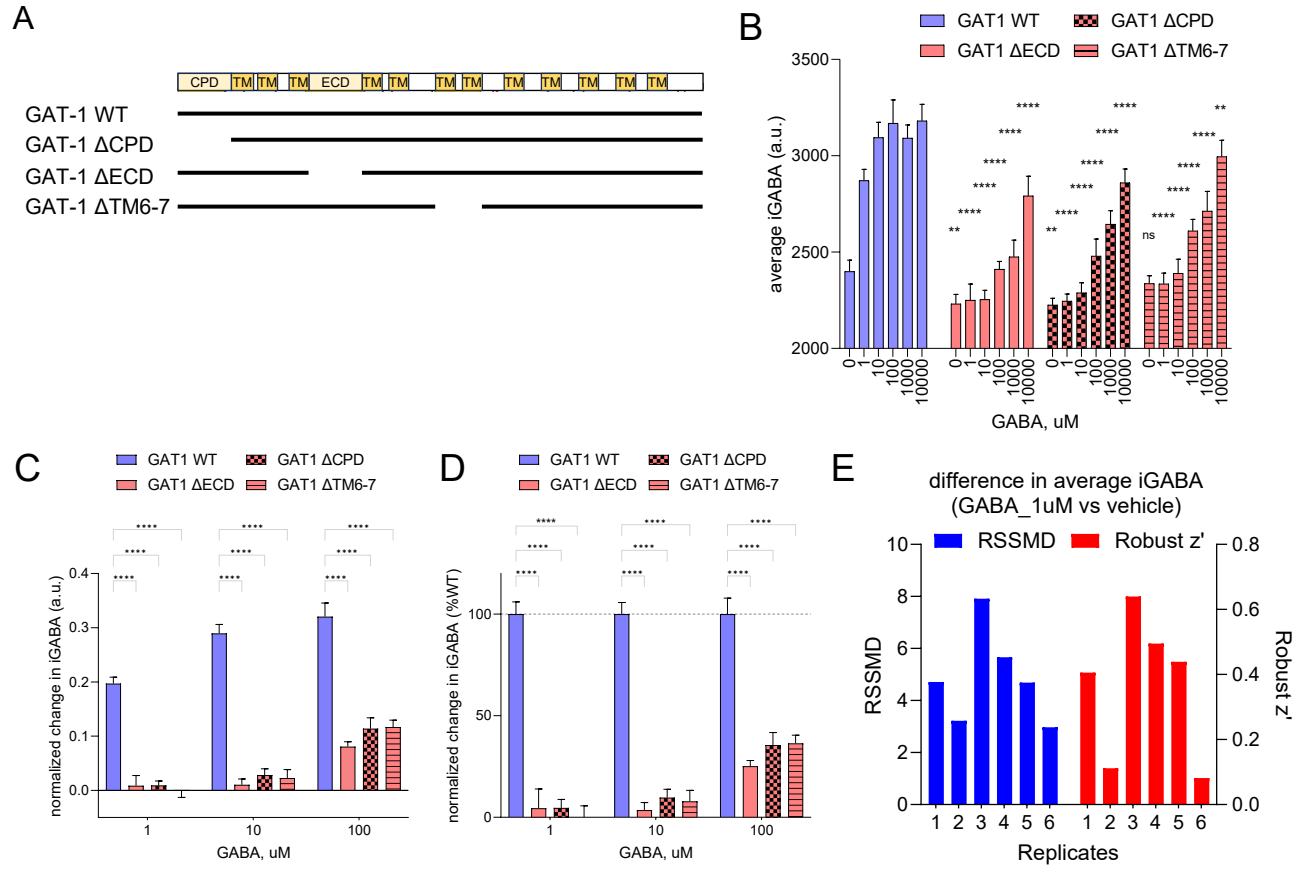
A
CPD
TM
ECD
GAT-1 WT
GAT-1 ΔCPD
GAT-1 ΔECD
GAT-1 ΔTM6-7
B
GAT1 WT
GAT1 ΔCPD
GAT1 ΔECD
GAT1 ΔTM6-7
average iGABA (a.u.)
GABA, uM
C
normalized change in iGABA (a.u.)
GABA, uM
D
normalized change in iGABA (%WT)
GABA, uM
E
difference in average iGABA
(GABA_1uM vs vehicle)
RSSMD
Robust z'
Replicates

Figure 3

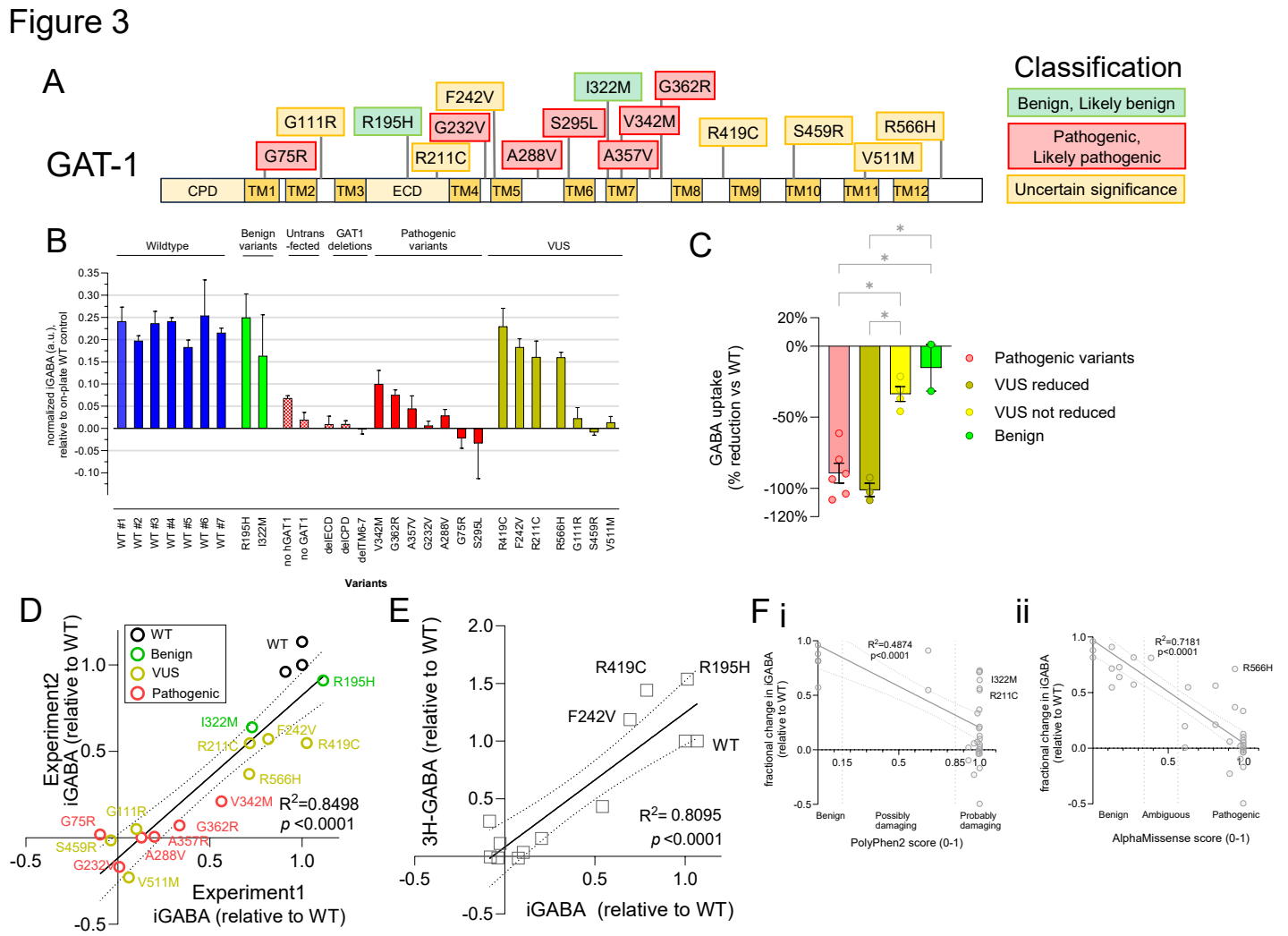
A
GAT-1
Classification
Benign, Likely benign
Pathogenic, Likely pathogenic
Uncertain significance
CPD
TM1
TM2
TM3
ECD
TM4
TM5
TM6
TM7
TM8
TM9
TM10
TM11
TM12
G75R
G111R
R195H
R211C
F242V
G232V
A288V
S295L
I322M
A357V
V342M
G362R
R419C
S459R
V511M
R566H
B
Wildtype
Benign variants
Untrans -fected
GAT1 deletions
Pathogenic variants
VUS
normalized iGABA (a.u.) relative to on-plate WT control
Variants
C
GABA uptake (% reduction vs WT)
Pathogenic variants
VUS reduced
VUS not reduced
Benign
D
WT
Benign
VUS
Pathogenic
Experiment2 iGABA (relative to WT)
Experiment1 iGABA (relative to WT)
R2=0.8498
p <0.0001
E
3H-GABA (relative to WT)
iGABA (relative to WT)
R2= 0.8095
p <0.0001
F i
ii
fractional change in iGABA (relative to WT)
R2=0.4874
p<0.0001
PolyPhen2 score (0-1)
Benign
Possibly damaging
Probably damaging
R2=0.7181
p<0.0001
AlphaMissense score (0-1)
Ambiguous
Pathogenic

Figure 4

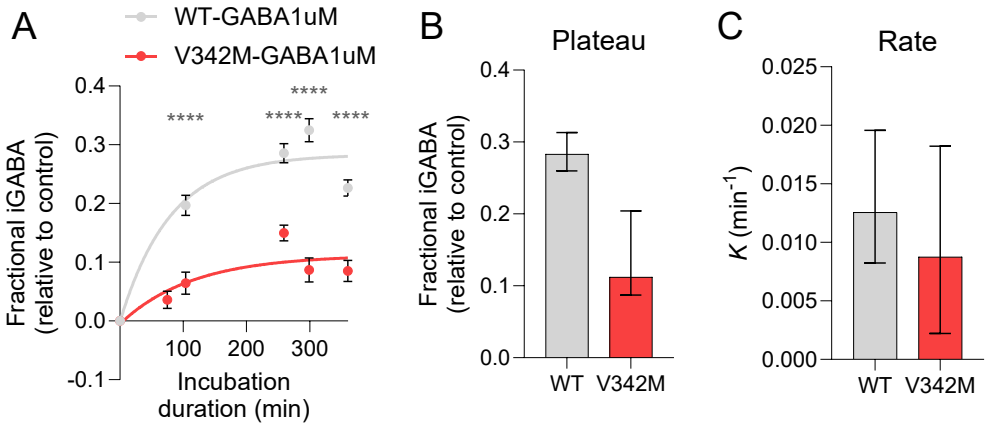
A
WT-GABA1uM
V342M-GABA1uM
Fractional iGABA (relative to control)
0.4
0.3
0.2
0.1
0.0
-0.1
****
****
****
****
100
200
300
Incubation duration (min)
B
Plateau
Fractional iGABA (relative to control)
0.4
0.3
0.2
0.1
0.0
WT
V342M
C
Rate
K (min-1)
0.025
0.020
0.015
0.010
0.005
0.000
WT
V342M

Figure 5

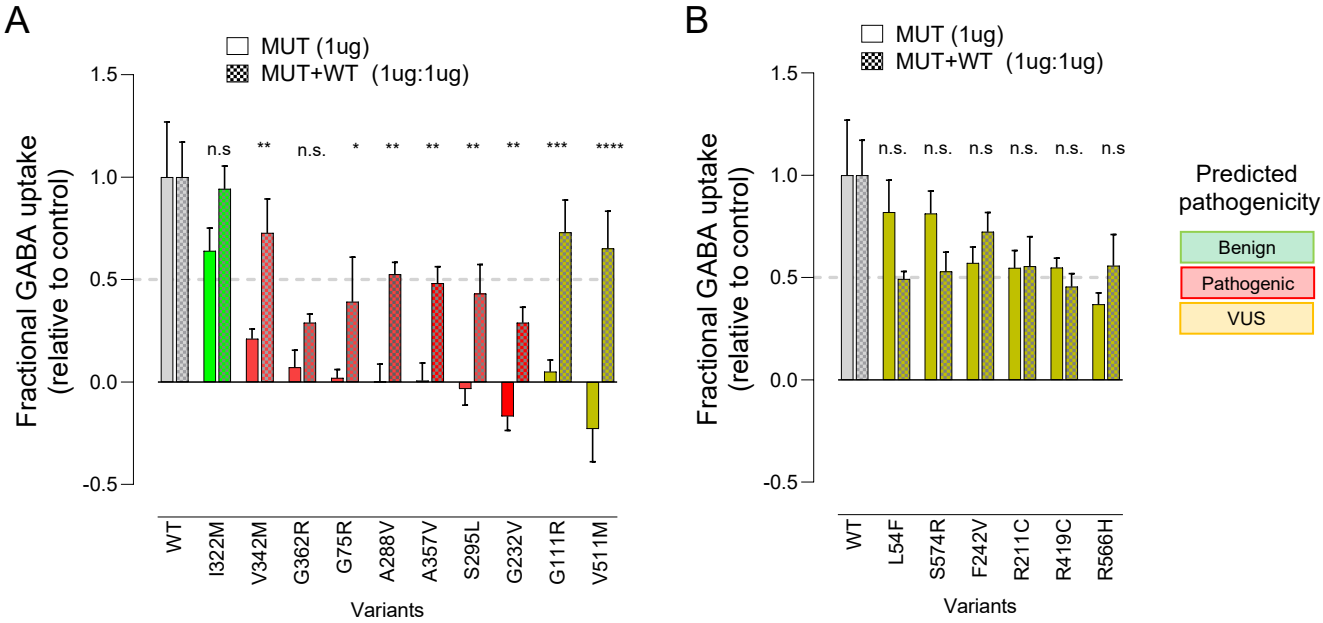
A
MUT (1ug)
MUT+WT (1ug:1ug)
Fractional GABA uptake (relative to control)
1.5
1.0
0.5
0.0
-0.5
n.s
**
n.s.
*
**
**
**
**
***
****
WT
I322M
V342M
G362R
G75R
A288V
A357V
S295L
G232V
G111R
V511M
Variants
B
MUT (1ug)
MUT+WT (1ug:1ug)
Fractional GABA uptake (relative to control)
1.5
1.0
0.5
0.0
-0.5
n.s.
n.s.
n.s
n.s.
n.s.
n.s
WT
L54F
S574R
F242V
R211C
R419C
R566H
Variants
Predicted pathogenicity
Benign
Pathogenic
VUS

Figure 6

A

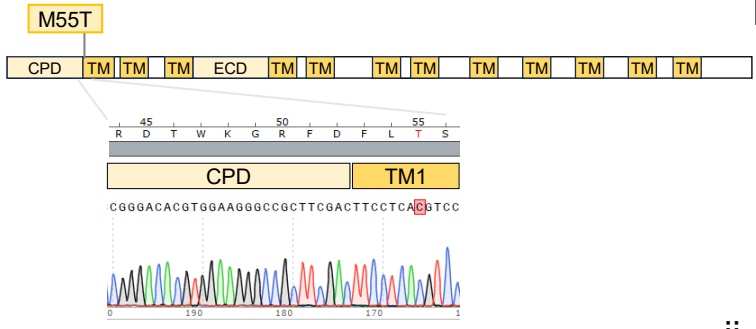

B

Functional prediction of GAT-1 p.M55T variant	
Revel	Deleterious (0.72)
AlphaMissense	Moderate (0.934)
MUT Assessor	Medium (2.32)
SIFT	Deleterious (0)
PolyPhen2	Benign (0.222)
MetaLR	Benign (low, 0.39)

C i

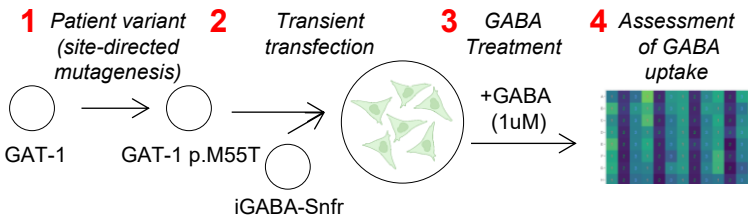

ii

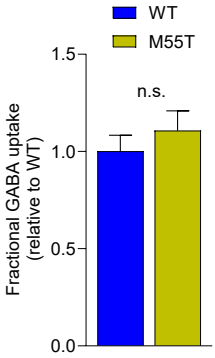

iii

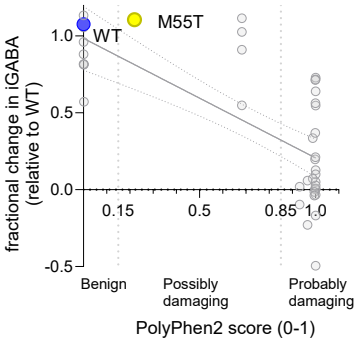

Figure 7

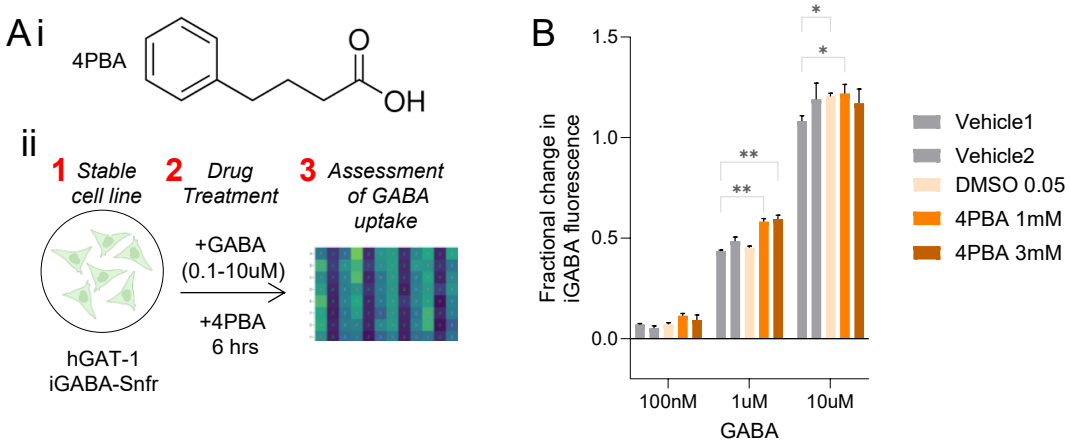
Ai
4PBA
O
OH
ii
1 Stable cell line
2 Drug Treatment
3 Assessment of GABA uptake
+GABA (0.1-10uM)
+4PBA 6 hrs
hGAT-1 iGABA-Snfr
B
Fractional change in iGABA fluorescence
1.5
1.0
0.5
0.0
**
**
*
*
100nM
1uM
10uM
GABA
Vehicle1
Vehicle2
DMSO 0.05
4PBA 1mM
4PBA 3mM

Figure 8

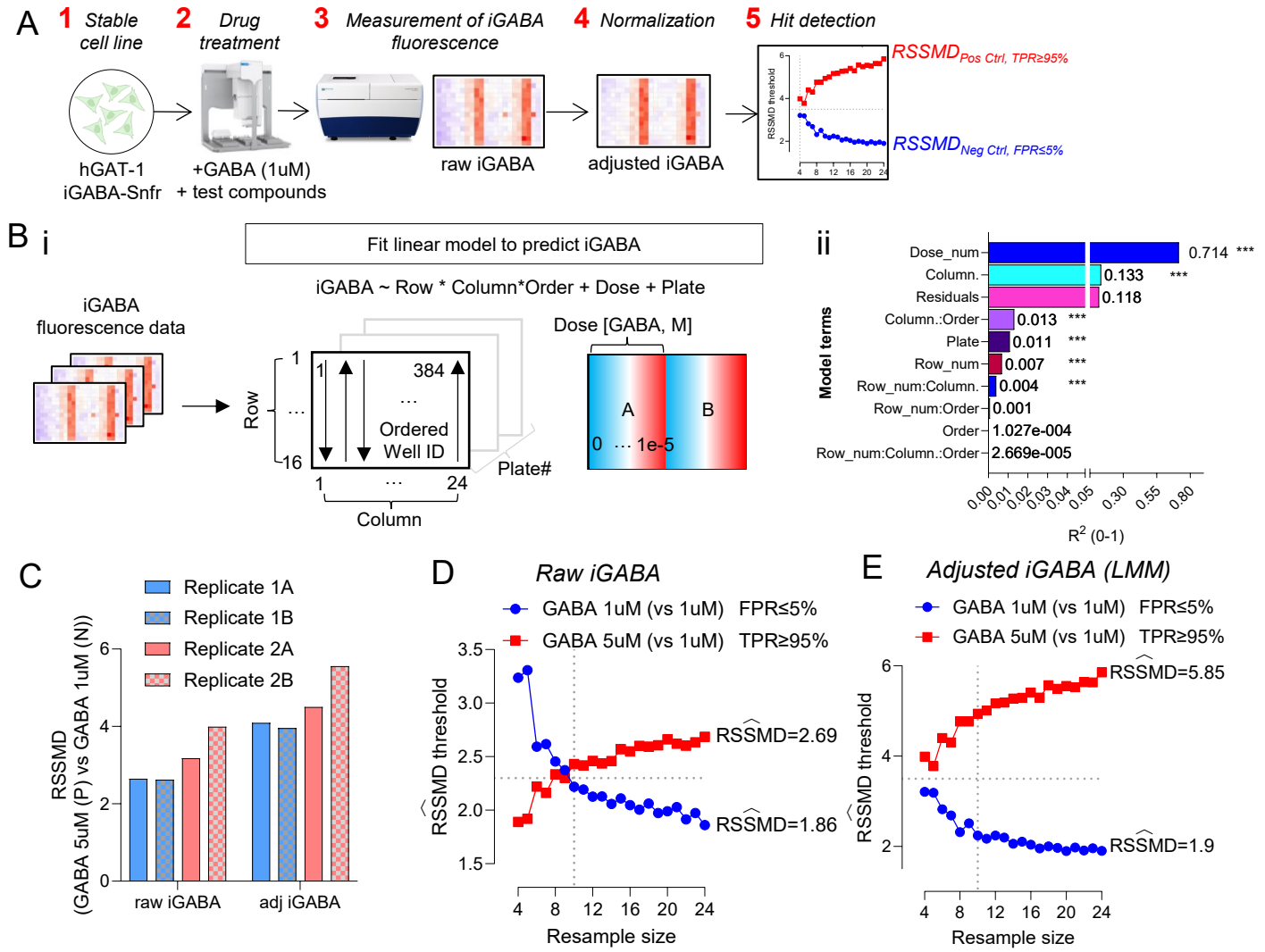
A
1 Stable cell line
2 Drug treatment
3 Measurement of iGABA fluorescence
4 Normalization
5 Hit detection
hGAT-1 iGABA-Snfr
+GABA (1uM) + test compounds
raw iGABA
adjusted iGABA
RSSMD threshold
RSSMD Pos Ctrl, TPR≥95%
RSSMD Neg Ctrl, FPR≤5%
B i
Fit linear model to predict iGABA
iGABA ~ Row * Column*Order + Dose + Plate
iGABA fluorescence data
Row
Ordered Well ID
Plate#
Column
Dose [GABA, M]
A
B
0 ... 1e-5
ii
Model terms
Dose_num 0.714 ***
Column. 0.133 ***
Residuals 0.118
Column.:Order 0.013 ***
Plate 0.011 ***
Row_num 0.007 ***
Row_num:Column. 0.004 ***
Row_num:Order 0.001
Order 1.027e-004
Row_num:Column.:Order 2.669e-005
R2 (0-1)
C
Replicate 1A
Replicate 1B
Replicate 2A
Replicate 2B
RSSMD (GABA 5uM (P) vs GABA 1uM (N))
raw iGABA
adj iGABA
D
Raw iGABA
GABA 1uM (vs 1uM) FPR≤5%
GABA 5uM (vs 1uM) TPR≥95%
RSSMD threshold
RSSMD=2.69
RSSMD=1.86
Resample size
E
Adjusted iGABA (LMM)
GABA 1uM (vs 1uM) FPR≤5%
GABA 5uM (vs 1uM) TPR≥95%
RSSMD threshold
RSSMD=5.85
RSSMD=1.9
Resample size

Table 1. Clinical and molecular characterization of GAT-1 variants investigated in this study.

Human variant		Variant name (dbSNP)	Consequence specific allele	Protein allele	Variant start (aa)	PolyPhen2 prediction	PolyPhen2	SIFT prediction	SIFT score	Variant supporting evidence	ClinVar or ACMG classification	Unique cases	% variant a/w epilepsy	iGABA fluorescence (%WT)
p.M55T	Met55Thr	rs2124905468	T/C	M/T	55	benign	0.22	deleterious	0	Phenotype_or_Disease, gnomAD	Uncertain significance	2	50% (1/2)	+10%
p.G75R	Gly75Arg	rs1064795852	G/A	G/R	75	possibly damaging	0.931	tolerated	0.05	Cited, Phenotype_or_Disease	Likely pathogenic / pathogenic	3	100% (3/3)	-103.9%
p.G111R	Gly111Arg	rs1559622516	G/A	G/R	111	probably damaging	1	deleterious	0	Phenotype_or_Disease	Conflicting interpretations (uncertain significance, likely pathogenic)	2	50% (1/2)	-92.5%
p.R195H	Arg195His	rs773445048	G/A	R/H	195	possibly damaging	0.682	tolerated	0.07	ExAC,Frequency, gnomAD, Phenotype_or_Disease, TOPMed	Benign	1	100% (1/1)	+1.3%
p.R211C	Arg211Cys	rs756927822	C/T	R/C	211	probably damaging	1	deleterious	0	ExAC,Frequency, gnomAD	Uncertain significance	1	0% (0/1)	-36.8%
p.G232V	Gly232Val	rs1697444014	G/T	G/V	232	probably damaging	1	deleterious	0	Phenotype_or_Disease	Likely pathogenic	4	75% (3/4)	-108%
p.F242V	Phe242Val	rs1399297934	T/G	F/V	242	benign	0.002	tolerated	0.1	Frequency,gnomAD, TOPMed	Uncertain significance	2	100% (2/2)	-30.6%
p.A288V	Ala288Val	rs794726860	C/T	A/V	288	probably damaging	1	deleterious	0	Cited, Phenotype_or_Disease	Likely pathogenic / pathogenic	7	71.4% (5/7)	-93.6%
p.S295L	Ser295Leu	rs1574907241	C/T	S/L	295	probably damaging	1	deleterious	0	Phenotype_or_Disease	Likely pathogenic*	1	0% (0/1)	-103.3%
p.I322M	Ile322Met	rs757627416	C/G	I/M	322	probably damaging	1	tolerated	0.33	ExAC,Frequency, gnomAD, TOPMed, Phenotype_or_Disease	Likely benign**, uncertain significance	1	100% (1/1)	-31.6%
p.V342M	Val342M	rs760836450	G/A	V/M	342	probably damaging	0.999	deleterious	0	Cited,ExAC,Frequency, gnomAD, Phenotype_or_Disease, TOPMed	Pathogenic	11	90.9% (10/11)	-61.3%
p.A357V	Ala357Val	rs1553689859	C/T	A/V	357	probably damaging	0.997	deleterious	0.02	Cited, Phenotype_or_Disease	Pathogenic	4	100% (4/4)	-89.8%
p.G362R	Gly362Arg	rs1131691302	G/A	G/R	362	probably damaging	0.987	deleterious	0	Cited, Phenotype_or_Disease	Likely pathogenic / pathogenic	3	100% (3/3)	-79.7%
p.R419C	Arg419Cys	rs910130675	C/T	R/C	419	possibly damaging	0.682	deleterious	0.01	Frequency,gnomAD, Phenotype_or_Disease, TOPMed	Uncertain significance	1	100% (1/1)	-21.3%
p.S459R	Ser459Arg	rs1064795099	C/A	S/R	459	probably damaging	0.994	deleterious	0.02	Cited, Phenotype_or_Disease	Conflicting interpretations (likely pathogenic, uncertain significance)	2	100% (2/2)	-102.6%
p.V511M	Val511Met	rs1064794981	G/A	V/M	511	probably damaging	0.965	tolerated	0.06	Cited, Phenotype_or_Disease	Conflicting interpretations (uncertain significance, likely pathogenic, pathogenic)	3	100% (3/3)	-108.5
p.R566H	Arg566His	rs767142926	G/A	R/H	566	probably damaging	0.998	deleterious	0	ExAC,Frequency, gnomAD, Phenotype_or_Disease	Uncertain significance	1	100% (1/1)	-45.9%

Data related to number of unique cases and prevalence of epilepsy were retrieved from SLC6A1 Portal (Sept 8, 2022). iGABA fluorescence values are the average of two independent experiments.
*, reported as “Uncertain Significance” in ClinVar, but “Likely pathogenic” supported by ACMG criteria due to PM1 (missense variant in mutational hot spot or well-defined domain), PP2 (missense variant in gene with low rate of benign missense variants), PM2 (extremely low frequency in gnomAD).
**, the variant is not present in ClinVar, but predicted “Likely benign” in Ensembl Variant Effect Predictor. By ACMG criteria, it is consistent with VUS due to PM2 (low frequency in gnomAD), PP2 (missense variant in gene with low rate of benign missense variants)

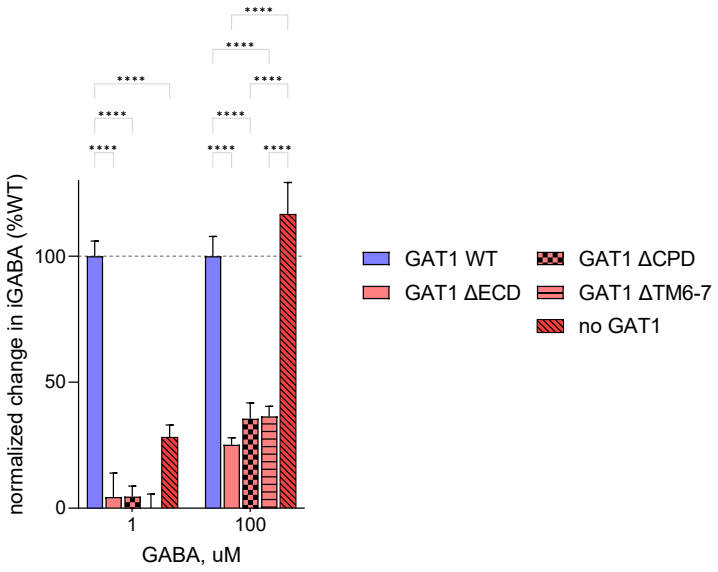

Supplementary Figure 1. Deletion constructs interfere with non-specific GABA uptake. Transfection of GAT-1 deletion mutants reduces GABA uptake relative to untransfected ("no GAT-1") control, particularly at higher extracellular GABA concentrations (100uM). Assay format is 96-well plate, transient transfection, incubation time 6-7 hrs. Data are the mean +/- SEM of independent per-well averages of iGABA (4 wells per condition (construct x GABA concentration), 4 sites per well). (Two-way ANOVA, with Tukey's comparison test. ****, $p<0.0001$)

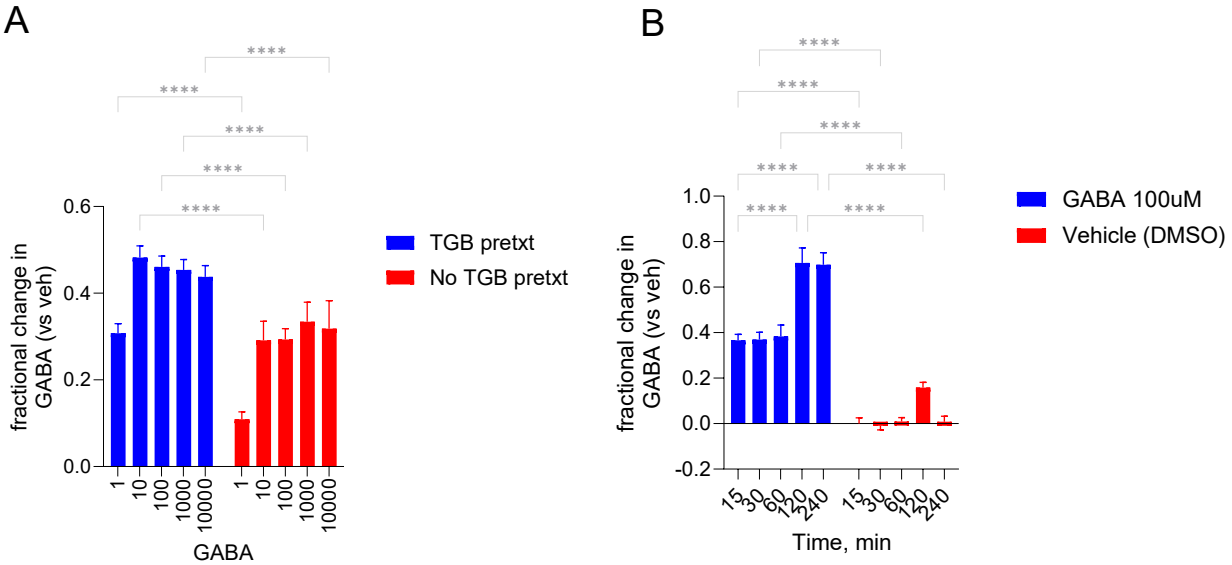

Supplementary Figure 2. Assay optimization. A) Overnight pretreatment with GAT-1 inhibitor (tiagabine) followed by wash-out increases fractional change in iGABA across all GABA concentrations tested. Statistics are ANOVA followed by Sidak's test (1 family, 5 comparisons, 1 per row (GABA); ****, $p<0.0001$. **B**) GABA fluorescence increases rapidly following incubation with GABA 100uM, but continues to increase at later timepoints (4 sites per well, 45 wells per condition). Statistics are ANOVA followed by Sidak's test (7 families, 1 comparison per row (GABA), 10 comparisons per column (Time); ****, $p<0.0001$.

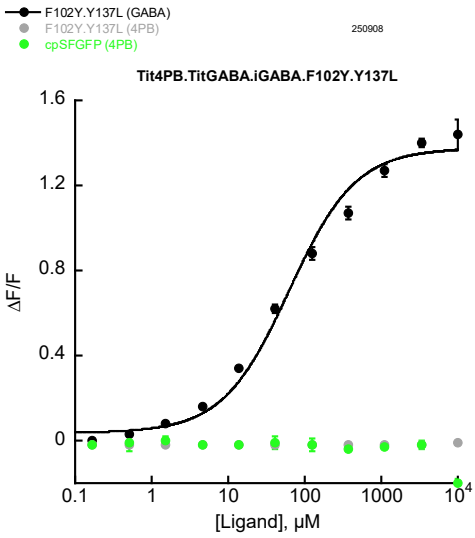

Supplementary Figure 3. No effect of 4-phenylbutyrate on iGABA-Snfr fluorescence. Data are average normalized fluorescence +/- S.D. (n= 3 replicates per condition) from iGABA-Snfr.F102Y.Y137L incubated with GABA (*black*) or 4-phenylbutyrate (4-PB; *grey*) across a 6-log range of ligand concentrations. Circularly permuted super-folder GFP with 4-PB (*green*) is shown as a control.

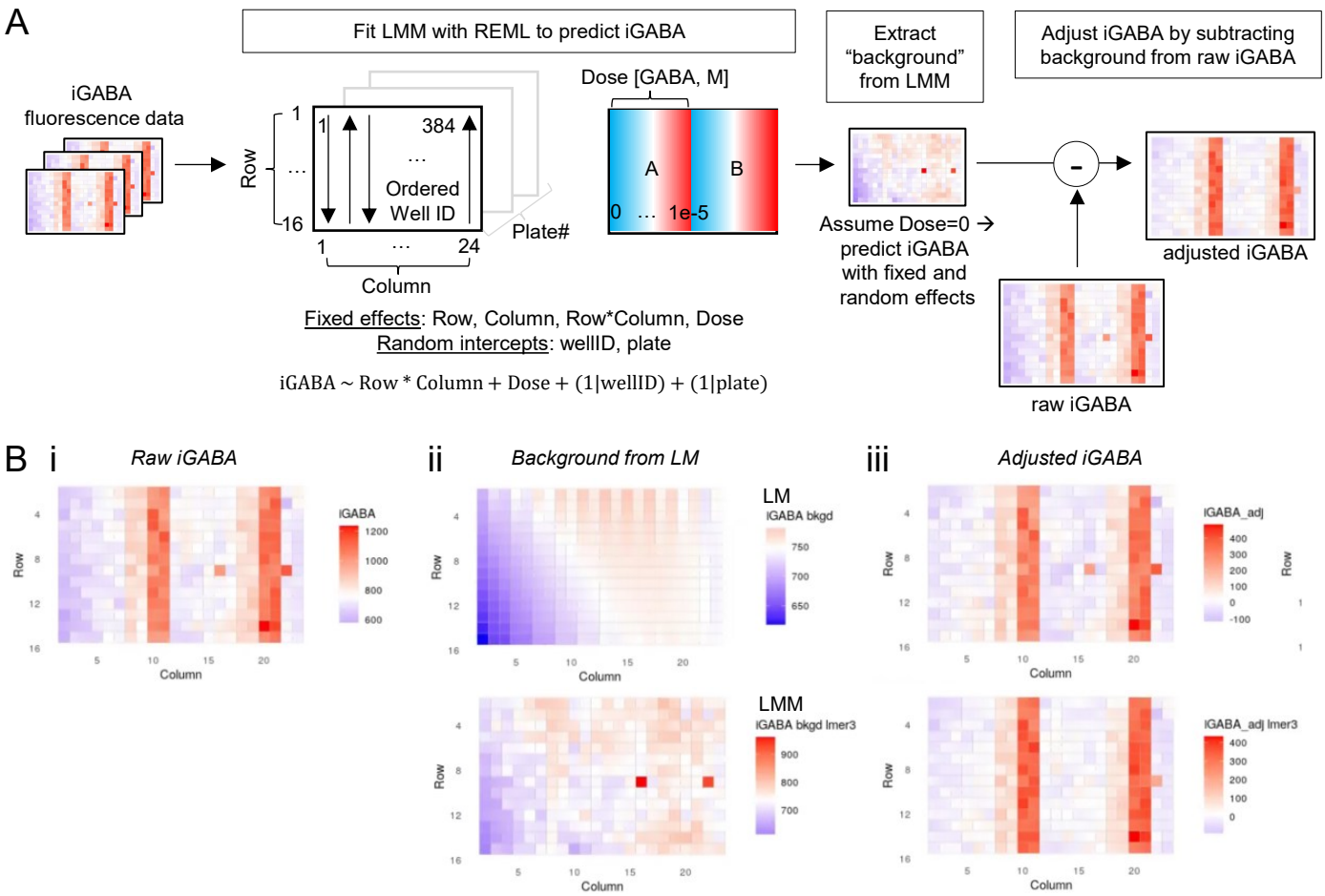

Supplementary Figure 4. Methods of plate normalization. (**A**) Approach to plate normalization based on linear mixed model (LMM). (**B**) Graphical representation of methods based on linear model vs LMM to extract background (ii) and adjust iGABA (iii).

Supplementary Table 1. Primers for mutagenesis

V006 M55T F	ttcctcaCgtcctgtgtgggctatgccatc
V006 M55T R	cacaggacGtgaggaagtcgaagcggc
V006 A357V F	atgtggTggcctcaggcccc
V006 A357V R	tgaggccAccacatcagcaatggacc
V006 G111R F	ctccatcCgggggctaggggtatggaagc
V006 G111R R	gcccccGgatggaggtgtactggcc
V006 G362R F	aggccccAggctggcgttcct
V006 G362R R	cgccagccTggggcctgag
V006 G75 R	tttttccTgcagagatagggaacctccagacg
V006 G75R F	ctctgcAggaaaaatggtgggggagcctt
V006 I322M F	ccatcatGgtctgctgcatcaattcgtgc
V006 I322M R	cagacCatgatggagtccctgtagac
V006 L54F F	gacttcTtcatgtcctgtgtgggctatgcca
V006 L54F R	acatgaAgaagtcgaagcggcccttccac
V006 R195H F	gggagcAcaacatgcatcagatgacggacg
V006 R195H R	atgttgTgctcccagaactccaccacag
V006 R211C F	tcagatcTgctggccactggcca
V006 R211C R	ggccagcAgatctgacctggcttatccagc
V006 R419C F	cgcaacTgcagagagctcttcattgct
V006 R419C R	ctctgcAgttgcggaggagcctgg
V006 S295L F	tcttctTatacgggctgggcctggg
V006 S295L R	cccgtatAagaagaagatctgggttgccgc
V006 S459R F	gcatgagGctgctgttcctcgtgttct
V006 S459R R	acagcagCctcatgccactggcagagtagt

V006 S574R F	gcccagGgaagacatcgttcgccca
V006 S574R R	gtcttcCctgggctggaccatgacttggat
V006 del TM6-7 F	gatgcggcaacccagggcttcatgg
V006 del TM6-7 R	ctgggttgccgcatccagccacac
V006 del-CPD F2	ATAGGgGCCaCCatgttcctcatgtcc
V006 del-CPD R2	catGGtGGCcCCTATAGTGAGTCGTATTAATTTCGA
V006 del-ECD F2	ctacatcgtcatcatctggccactggcc
V006 del-ECD R	gatgatgacgatgtagtagatgttcagccagaatgatagcac
V006 A288V F	ctggatgTggcaacccagatcttcttctcat
V006 A288V R	ggttgccAcatccagccacacctc
V006 F242V F	tggtctacGtttcagccacatacccctacatcat
V006 F242V R	ctgaaaCgtagaccacctttccagtccagccaa
V006 G232V F	ctggaaggTtgttggctggactggaaag
V006 G232V R	ccaacaAccttccagatacagaaatacacaaggatcca
V006 K448R F	tcttcaGactctttgactactactctgccagtggc
V006 K448R R	caaagagtCtgaagacataaatacccccctgagtgatgt
V006 R566H F	aagcagcAcatccaagtcatggtcca
V006 R566H R	ttggatgTgctgcttcagggagc
V006 V342M F	tccatcAtgggcttcatggcccatgt
V006 V342M R	tgaagcccaTgatggagaagatgacgaatc
V006 V511M F	ggcgggcAtgttcattttcagtgctgtgc
V006 V511M R	atgaacaTgcccgccacaatgattggtgt